Redox Biology 36 (2020) 101672

Contents lists available at ScienceDirect

Redox Biology

journal homepage: www.elsevier.com/locate/redox

Increases of iASPP-Keap1 interaction mediated by syringin enhance synaptic plasticity and rescue cognitive impairments *via* stabilizing Nrf2 in Alzheimer's models

Chun-Yan Wang [a,b,*], Qi Zhang [a], Zhe Xun [a], Lin Yuan [a], Ruonan Li [a], Xiang Li [a], Shu-Yu Tian [a], Na Xin [a,1], Ye Xu [b]

[a] Institute of Health Sciences, Key Laboratory of Medical Cell Biology of Ministry of Education, China Medical University, Shenyang, 110122, China
[b] Translational Medicine Laboratory, Basic College of Medicine, Jilin Medical University, Jilin, 132013, China

ARTICLE INFO

Keywords:
Alzheimer's disease
Oxidative stress
iASPP/Nrf2 axis
Syringin
Synaptic plasticity
Amyloid pathology

ABSTRACT

Oxidative stress is an important pathogenic manifestation of Alzheimer's disease (AD) that contributes to synaptic dysfunction, which precedes Aβ accumulation and neurofibrillary tangle formation. However, the molecular machineries that govern the decline of antioxidative defence in AD remains to be elucidated, and effective candidate for AD treatment is limited. Here, we showed that the decreases in the inhibitor of apoptosis-stimulating protein of p53 (iASPP) was associated with the vulnerability to oxidative stress in the amyloid precursor protein (APP)/presenilin 1 (PS1) mouse brain. Treatment with an antioxidant, syringin, could ameliorate AD-related pathologic and behavioural impairments. Interestingly, syringin treatment resulted in an upregulation of iASPP and the increase in the interaction of iASPP with Kelchlike ECH-associating protein 1 (Keap1). Syringin reduced neuronal apoptosis independently of p53. We confirmed that syringin-induced enhancement of antioxidant defenses involved the stabilization of Nrf2 in overexpressing human Swedish mutant APP (APPswe) cells *in vitro*. Syringin-mediated Nrf2 nuclear translocation facilitated the activation of the Nrf2 downstream genes *via* iASPP/Nrf2 axis. Our results demonstrate that syringin-mediated increases of iASPP-Keap1 interaction restore cellular redox balance. Further study on the syringin-iASPP interactions may help in understanding the regulatory mechanism and designing novel potent modulators for AD treatment.

1. Introduction

Alzheimer's disease (AD) is a chronic neurodegenerative disease and the most common form of age-related dementia, which has become a global health and social problem with the ageing of the world's population. The clinical characteristics of AD patients are progressive cognition impairment accompanied by the pathological features of decreased synaptic density, neuronal dysfunction and neuronal loss in the hippocampus and cortex of the basal forebrain. Various genetic, age-related and environmental factors are generally accepted to be related to the initiation and progression of AD, although the causes of AD remain unknown. Chronic exposure to oxidative imbalance and degenerative processes modulate the magnitude and severity of AD [1].

Considering the roles of oxidative stress, misfolded proteins and inflammation in AD progression [2–4], the mechanism by which nuclear factor erythroid 2-related factor 2 (Nrf2) is downregulated in the AD brain and the effects of boosting its expression are important areas of investigation. Nrf2 is a transcription factor that regulates various sets of adaptive responses to endogenous and exogenous stresses, neutralizing reactive oxygen species (ROS) and restoring cellular redox balance [5]. Under physiological conditions, the activity of Nrf2 is restricted by the binding of Kelchlike ECH-associating protein 1 (Keap1) in the cytoplasm [6] and is ubiquitinated and degraded by the ubiquitin-proteasome system [7]. Upon oxidative status, Nrf2 is not bound to Keap1 and undergoes nuclear translocation. Nrf2 then binds to small Maf proteins, resulting in the binding of Nrf2 to antioxidant responsive elements (AREs) within the promoter regions of a series of genes encoding antioxidant enzymes and cellular defence targets [8,9]. However, the

* Corresponding author. Key Laboratory of Medical Cell Biology of Ministry of Education of China Institute of Health Sciences, China Medical University, No.77 Puhe Road, Shenyang North New Area, Shenyang, China.
E-mail address: wangchunyan@cmu.edu.cn (C.-Y. Wang).
[1] Chun-Yan Wang, Qi Zhang and Zhe Xun contributed equally to this work.

https://doi.org/10.1016/j.redox.2020.101672
Received 15 June 2020; Received in revised form 15 July 2020; Accepted 3 August 2020
Available online 10 August 2020

protein expression of nuclear Nrf2 is reduced in the hippocampus and frontal cortex of the AD postmortem brain [10]. Downregulation of Nrf2 signalling has also been observed in the brain of an AD mouse model [11]. Kanninen and colleagues reported that lentiviral vector-mediated Nrf2 elevation in the APP/PS1 mouse brain improved spatial learning [12]. We previously observed that the upregulation of Nrf2 caused by antioxidant treatment enhanced thioredoxin-1 (TrX) activity, inhibited NLRP3 inflammasome formation and ameliorated neuronal apoptosis in the APP/PS1 mouse brain [13]. However, the precise molecular machineries that govern the Nrf2 decline in AD development remain unclear.

The inhibitor of apoptosis-stimulating protein of p53 (iASPP), a member of the ASPP family, has attracted much attention because of its effects on p53 apoptotic regulation. The ASPP family comprises three members, namely, ASPP1, ASPP2 and iASPP. ASPP1 and ASPP2 are activators of p53 that bind with p53 to enhance p53-induced apoptosis of DNA-damaged cells [14,15]. In contrast, iASPP interacts with p53 to inhibit the ability of p53 to transactivate proapoptotic target genes [15,16]. Several studies have shown that enhanced expression of iASPP is related to cancers [17–19]. iASPP protein expression was reported to be remarkably reduced in a mouse model of focal cerebral ischaemia [20]. Liu and colleagues observed that iASPP is required for retinal ganglion cell survival after axonal damage [21]. Upregulating iASPP protein levels has been shown to protect the brain from ischaemia/reperfusion brain injury [22], whereas iASPP inhibition deteriorated oxidative stress damage in the neuronal cell line neuro-2a (N2a) *in vitro* [23]. Interestingly, Ge and colleagues reported that iASPP promoted Nrf2 accumulation and nuclear translocation by competing with Nrf2 for Keap1 in renal cell carcinoma [24]. Furthermore, iASPP-mediated decreases in ROS in renal cell carcinoma and bladder cancer cells were Nrf2 signalling-dependent [24]. However, the role of iASPP in AD is not well elucidated.

Syringin, 4-[(1E)-3-hydroxyprop-1-en-1-yl]-2,6-dimethoxyphenyl β-D-glucopyranoside], also known as eleutheroside B, the main active ingredient extracted from the rhizome and root of Eleutherococcus senticosus, has attracted attention because of its pharmacologic effects. Eleutherococcus senticosus has a long history of being widely used as a medicinal herb in Chinese medicine. The Chinese Pharmacopoeia (Pharmacopoeia, 2015) reports that senticosus was traditionally applied to treat kidney deficiency. Eleutheroside B possesses antioxidant activities [25]. Intravenous injection of syringin has been shown to lead to a decrease in plasma glucose levels in streptozotocin-induced diabetic rats [26]. Meanwhile, syringin treatment was also shown to attenuate insulin resistance caused by a high-fat diet in mice [27]. Syringin exhibited hepatoprotective effects in a mouse model of hepatic failure [28]. Liu and colleagues observed that syringin treatment prevented bone loss in ovariectomized mice [29]. Eleutheroside B or E improved learning and memory in a rat model of aging induced by quinolinic acid hippocampal injection [30]. Finally, syringin treatment reduced Aβ (25–35)-induced apoptosis *in vitro* [31]. However, to date, there is no comprehensive description about the effects of syringin on AD *in vivo*.

In the present study, we investigated the effects of syringin on the neuropathology of APP/PS1 double transgenic AD mice and identified its mechanism of action. The downregulation of iASPP in the APP/PS1 mouse brain was accompanied by decreases in nuclear Nrf2 levels. Syringin-induced increases in iASPP protein expression alleviated oxidative stress and mitigated synaptic deficiency in the APP/PS1 mouse brain. We show for the first time that iASPP impairment might be involved in the redox imbalance and cellular apoptosis in amyloid-related pathology. Our findings demonstrate the multitarget neuroprotective effects of syringin and suggest that syringin might be a potential therapeutic agent for AD treatment.

2. Materials and methods

2.1. Object and treatments

2.1.1. Animals and treatments

The APP/PS1 (B6C3-Tg [APPswe, PSEN1dE9] 85Dbo/Mmjax) double transgenic mice used as the AD animal model in the present study were obtained from Jackson Laboratory (West Grove, PA). Age-matched C57BL/6 mice provided by Jackson Laboratory were used as the wild-type (WT) controls. Four-month-old male APP/PS1 mice and age-matched WT mice were randomly divided into three groups: the control group treated with vehicle (150 μL), composed of 5% ethanol, 15% polyethylene glycol (PEG400) and 15% 1,2-propanediol in deionized water, and the syringin-administered groups treated with vehicle and syringin at doses of 20 and 60 mg/kg body weight. The mice were treated with vehicle or syringin by oral gavage once a day for five months. The body weight and general behaviour of the mice were monitored daily. Twenty-four hours after the last syringin or vehicle administration, mice were analysed using cognition-related behavioural tests. Our study was performed in accordance with the recommendations of "Laboratory Animals-Guideline of Welfare and Ethics, the Ethics Committee for Medical Laboratory Animals of China Medical University". The protocol was approved by the Ethics Committee for Medical Laboratory Animals of China Medical University (CMU2020003).

2.1.2. Cell culture and drug treatment

N2a cells or N2a cells overexpressing human Swedish mutant APP (APPswe) were grown in DMEM containing 10% FBS, 100 U/mL penicillin, 100 μg/mL streptomycin in a fully humidified, 5% CO_2 incubator at 37 °C. APPswe cells were with addition of G418 (200 μg/mL). Once the cells grew to 80% confluence, they were exposed to fresh serum-free medium. The cells were then treated with H_2O_2, syringin, small interfering RNA (siRNA) targeting iASPP or Nrf2 using Lipofectamine 2000, or the Nrf2 inhibitor, trigonelline, as indicated. Culture cells treated with vehicle were used as controls.

2.2. Behavioural testing

A novel object recognition test (NORT) was carried out as previously described [32] to investigate the recognition memory of the APP/PS1 mice and age-matched WT mice. During the first two days, the mice were placed into the arena and allowed to habituate to the room for 10 min, twice per day. On the third day, two plastic blocks of identical volume were placed into the room. The blocks were sufficiently heavy and tall that the mice were unable to move or climb over them. The mouse was exposed to the two objects for 5 min. After that, the mouse was allowed to explore each of the two objects for 5 min to test short-term memory. The mice were given 5 min to test each of the two objects. During the 5-min intervals, one of the objects was replaced by a novel plastic cylinder. Then, the mouse was placed back into the room centre. The object exploration behaviour of the mouse was monitored and recorded by a digital pickup camera suspended above the arena. For long-term memory evaluation, the types of objects were altered, and the retention intervals were changed to 24 h. The acts of mouse directing the nose to within 2 cm from the object or touching the object using the nose and/or forepaws were defined as exploration behaviour. The discrimination index is the percentage of time spent exploring the novel object relative to the total time spent in both objects.

Morris water maze (MWM) tests were used to evaluate the recognition memory and spatial learning ability of the mice as previously described [33]. After two days of training on the location of the visible platform, the mice underwent a five-day navigation test to find the platform submerged 1 cm below the surface of the water. Every day, the mouse was subjected to three tests, and each test lasted a maximum of 1 min with a 1-min intertrial interval. The escape latency and the length of the path to the platform at each trial were acquired using a video

tracking system suspended above the tank. On the eighth day, the platform was removed. A probe trial was given to each mouse to determine its search bias. The mouse was allowed to swim in the tank for 60 s. The number of times the mouse crossed the place in which the platform had previously been located was recorded.

2.3. Electrophysiological recordings

After the behavioural tests, the mice were intraperitoneally anaesthetized with sodium pentobarbital (50 mg/kg). Blood samples of the mice were collected by their eyes, and the mice were sacrificed by immediate removal of the brain.

Hippocampal slices (400 μm) were kept in an interface chamber and perfused with oxygenated artificial cerebrospinal fluid [34]. To evoke the action of Shaffer-collateral and commissural fibres, bipolar tungsten stimulating electrodes were collated in the CA1 stratum radiatum. Extracellular field excitatory postsynaptic potentials (fEPSPs) were recorded with a glass microelectrode positioned in the vicinity of CA1 pyramidal neurons. Input/output curves were built *via* the variation of the stimulus current in steps of 50 μA (100–350 μA). Baseline fEPSPs were inducted with 2 0.1-ms pulses *per* minute at a pulse intensity adjusted to illicit fEPSPs at approximately 30%–50% of maximum. Paired pulse facilitation was examined to assess presynaptic function. Long-term potentiation (LTP) was elicited by high-frequency stimulation (HFS) by applying 4 × 150-Hz stimulus trains with 1-s pulses at 5-min intervals once stable basal EPSP responses had been recorded for 30 min. LTP is presented as the percentage of the average fEPSP slope.

2.4. Immunostaining

Serial 6-μm-thick coronal sections of frozen mouse brain were prepared. To assess the AD-like morphological alterations of the mouse brain, the sections were incubated with a mouse anti-Aβ antibody at 4 °C overnight after treatment with 3% normal donkey serum for 30 min. After the tissue underwent several washes, the specimens were co-incubated with Alexa Fluor 488-conjugated AffiniPure donkey anti-mouse IgG for 2 h at room temperature. To evaluate the distribution and expression of iASPP, we treated the brain slices with rabbit anti-iASPP antibody. Cy3-conjugated AffiniPure donkey anti-rabbit IgG was served as the secondary antibody. Rabbit anti-Nrf2 antibody was used to probe the protein expression of Nrf2 by immunohistochemistry. The brain sections were incubated with biotinylated goat anti-rabbit IgG, followed by amplification with streptavidin peroxidase. After treated with 0.025% 3,3-diaminobenzidine plus 0.0033% H_2O_2, the slices were covered with neutral balsam. The immunoreactivities of fluorescence labelling or immunohistochemistry staining were respectively examined by confocal laser-scanning microscope and light microscope.

2.5. Nissl staining

Frozen slices from mouse brains were treated with 0.1% cresyl violet at 37 °C for 20 min. After thorough rinsing, the stained sections were dehydrated with a graded series of ethanol solutions. Following clearing with xylene, the slices were mounted with neutral balsam and examined with a microscope. The neuronal cells with round and pale nuclear staining were considered surviving cells. Six brain slices per mouse were selected and subjected to quantification.

2.6. Apoptosis analysis

After perfusion with precooling saline, the mice were sacrificed. Hippocampal tissues of the mice were harvested and then minced with scissors. The fragments were lysed in 30 mg/mL papain for 30 min followed by 21% deoxyribonuclease I at 37 °C for 30 min [35,36]. After filtered through a 70-μm of mesh screen, the samples were washed with physiological saline (PBS) and then resuspended with separating buffer (20% Percoll in Hanks' balanced salt solution). The cells were collected by centrifugation at 400*g* for 10 min (room temperature). After rinsing with ice-cold buffer containing 10 mM HEPES, 140 mM NaCl, and 2.5 mM $CaCl_2$ (pH 7.4), the samples were then treated with binding buffer containing 5 μL of Annexin V-fluorescein isothiocyanate (FITC) plus 5 μL of propidium iodide (PI) for 15 min at 22 °C away from light. The apoptosis was determined using the FITC (FL1) fluorescence signal detectors.

2.7. Assessment of oxidative-redox status

2.7.1. Analysis of the reduced glutathione (GSH) to oxidative glutathione (GSSG) ratio

To assess the oxidative-redox status in the mouse brain, the levels of GSH and GSSG were measured as previously described [37]. Briefly, the brain tissues were homogenized using a 1:10 dilution of ice-cold PBS (pH 7.0) supplemented with a protease inhibitor cocktail. After centrifugation, the supernatant was collected. The levels of GSH and GSSG were measured with a GSH/GSSG detection kit per the manufacturer's instructions. The GSH/GSSG ratio was quantified.

2.7.2. Determination of glutathione peroxidase (GPX) and glutathione reductase (GR) activity

The activities of GPX and GR were analysed by colorimetric and ultraviolet colorimetric methods according to the manufacturer's protocol using GPX and GR assay kits. The absorbances were recorded at 412 nm and 340 nm, respectively.

2.7.3. ROS measurement

ROS contents in the brain tissue were measured as previously described [33]. Briefly, specimens were lysed with precooling lysis buffer (pH 7.4) containing 10 mM Tris-HCl, 100 mM sucrose, and 10 mM EDTA. After centrifugation, the samples were suspended in PBS and adjusted to a density of 2×10^6 cells/mL. Cells were incubated with HEPES-Tris buffer (pH 7.4) composed of l μM CM-H2DCFDA, 10 mM HEPES, 132 mM NaCl, 4.2 mM KCl, 1 mM $CaCl_2$ and 1 mM $MgCl_2$, away from light for 30 min. After several rinses, the specimens were collected by centrifugation and incubated in HEPES-Tris buffer for 10 min. Following lysis in lysis medium (1% Nonidet P-40, 150 mM NaCl and 50 mM Tris, pH 8.0), the samples were collected and diluted with deionized water. The fluorescence signals of the specimens were measured with a spectrometer at 490 nm using a VersaFluor Fluorometer System. *In vivo* evaluation of total superoxide levels [38] in the mouse brains were determined using dihydroethidium (DHE) stains as previously described with modification [39]. Briefly, 24 h after behavioural testing, the mice were given DHE (20 mg/kg) by two serial intraperitoneal injections at 1 h-intervals for 2 h. After the last injection, brains tissue were collected for subsequent immunostaining.

2.7.4. Mitochondrial superoxide detection

Fresh brain tissues from the mice were homogenized with ice-cold lysis buffer (10 mM Tris-HCl, 100 mM sucrose, 10 mM EDTA; pH 7.4). The cells were collected and incubated with 5 μM MitoSOX Red mitochondrial superoxide indicator according to the manufacturer's protocol for 10 min at 37 °C, protected from light. Then, the samples were gently washed three times with warm PBS buffer. The MitoSOX Red reagent oxidized by superoxide exhibits red fluorescence, the levels of which were measured by flow cytometric analyses.

2.8. Sandwich ELISA

8-Isoprostane, a marker of oxidative stress present in the blood, was evaluated. Briefly, blood was collected in a vacutainer containing 2.5% sodium citrate and subjected to alkaline hydrolysis. The samples were first incubated with 15% KOH at 4 °C for 60 min. The samples were then

neutralized by the addition of 10 times the volume of potassium phosphate buffer (pH 7.4). Ethanol was added to the mixtures to precipitate the protein. The supernatants were collected and evaporated by vacuum centrifugation, and the samples were resuspended in 1 M acetate buffer (pH 4.0). Total plasma 8-isoprostane was assayed using an EIA-based kit (Cayman Chemical, USA) according to the manufacturer's protocol.

Soluble human Aβ1-40 and Aβ1-42 levels were analysed as previously described [40]. The brain tissues from APP/PS1 mouse brains were homogenized in ice-cold 20 mM Tris (pH 8.5) with the addition of the protease inhibitor cocktail. After centrifugation, the supernatant was collected for the Aβ assays. To assess the Aβ secretion of APPswe cells *in vitro*, the culture medium of cells given the indicated treatment was collected. The Aβ1-40 and Aβ1-42 levels were assayed with appropriate Aβ ELISA kits (Invitrogen) in accordance with the manufacturer's protocol. The absorbance of the samples was determined at 450 nm with a 96-well plate reader.

2.9. Western blot analysis

Cells or brain tissue samples were lysed in RIPA buffer (pH 8.0) containing a protein protease inhibitor cocktail. The protein levels were determined using a BCA protein assay kit. Thirty micrograms of protein were separated with 10% sodium dodecyl sulfate polyacrylamide gels. After incubated with primary antibodies, the immunoblots were thoroughly washed with TBST, and were treated in appropriate species of HRP-conjugated secondary antibodies. The immune complex was visualized using an enhanced chemiluminescence (ECL) kit.

2.10. Co-immunoprecipitation assays

To assess the endogenous interaction between iASPP and Keap1, we collected protein (1 μg) from mouse brain tissues and cell lysates. The specimens were pre-cleaned using protein G-Sepharose as previously described [24]. The mixtures were treated with an antibody against iASPP at 4 °C overnight. Immune complexes were collected and thoroughly washed using immunoprecipitation lysis buffer with the addition of a protease inhibitor cocktail. The precipitates were collected, boiled for 5 min and analysed by Western blot analyses with anti-p53 or anti-Keap1 antibodies.

2.11. Flow cytometry

Furthermore, to assess the cell cycle, we performed propidium iodide uptake analyses. After the indicated treatments, the cultured cells were collected and treated with RNase. The cultured cells were then incubated in precooled PI (1 mg/mL) away from light for 30 min at 4 °C. The stained cells were quantified by flow cytometry with gating of the cell population of interest according to the forward- and side-scatter features. The vertical and horizontal lines were devised on the basis of the autofluorescence of untreated cells. For apoptosis detection, the cells were prepared by trypsinization from the tissue of mouse brains. The cells were harvested by centrifugation and resuspended in PBS. Then, the cells from tissues or cultured cells were treated with ice-cold 75% ethanol for 1 h. The cells in early and late apoptosis were assessed using the Annexin V- FITC/PI kit. The cells were incubated with binding buffer (5 μL Annexin V-FITC and 5 μL PI) at room temperature for 15 min, protected from light, and analysed by FITC (FL1) and PI (FL2) signal detectors.

2.12. Cell fraction and DNA-binding activity analyses

The cytoplasm and nuclei of the cells were separated with a nuclear extract kit as previously described with minor modifications [41]. Briefly, the cells were homogenized in precooled lysis buffer. After centrifugation, the supernatant was obtained as the cytosolic fraction. The pellets were washed with lysis buffer supplemented with 40 μL of 10% Nonidet (NP-40) and underwent homogenization again. The precipitates were resuspended in the precooled nuclear fraction buffer. After centrifugation at 14,000 *g* for 5 min at 4 °C, the resultant supernatant containing nuclear proteins was obtained. The DNA-binding activities of Nrf2 and p53 in the nuclear extracts were measured with the TransAM Nrf2 and TransAM p53 Kits, respectively. The absorbance was quantified at 450 nm.

2.13. Real-time PCR

Total RNA was extracted from cerebral cortex tissue or cultured cells using an RNA isolation kit in accordance with the manufacturer's instructions. A total of 2 μg of RNA was used for reverse transcription with the Prime Script RT Reagent Kit. The cDNA synthesis conditions were 37 °C for 15 min and then 85 °C for 5 s. Quantitative real-time PCR was performed as previously described [33] in the 7300 Sequence Detection System using the SYBR Green PCR Master mix. At least three independent assays of each cDNA sample were conducted. The primers and probes used in PCR are listed in Supplementary Table 1. The expression levels were expressed as the ratio of threshold cycle (Ct) values to β-actin. The relative differences between the treatment group and control group were represented as a percentage compared to control.

2.14. Chromatin immunoprecipitation (ChIP) assays

Chromatin immunoprecipitation assays were performed as previously described [42]. Briefly, the brain tissue of the mice that underwent fixation with 4% paraformaldehyde was neutralized with 0.125 M glycine at 4 °C for 10 min. The specimens were washed using PBS and homogenized in lysis buffer (0.1% SDS, 0.5% Triton X-100, 20-mM Tris-HCl, 150-mM NaCl, pH 8.1) plus a protease inhibitor complex. Nuclear protein was collected by centrifugation, and one-third of it was kept as the input genomic DNA control. The remaining nuclear proteins were treated with antibodies against p53 or nonimmune IgG (negative control) for 18 h at 4 °C. Then, the protein-DNA complexes were captured by protein A-agarose beads. After thorough rinses, the pellets were treated with elution buffer (pH 8.0). The beads were collected by centrifugation and treated with 5-M NaCl to reverse formaldehyde cross-links. The samples were heated at 65 °C for 12 h. Protein-DNA complexes were then deproteinated using 20 mg/mL proteinase K at 45 °C for 1 h. After purification, the DNA was used for amplification. Real-time PCR was performed with the primers for the p53-dependent genes, Bax and p53 upregulated modulator of apoptosis (PUMA).

2.15. Statistical analysis

Data are expressed as the means ± standard error of the mean (S.E.M.). Repeated measures analysis of variance (ANOVA), one-way or two-way ANOVA was applied to evaluate the statistical significance. The genotype × treatment interactions, together with the main effect of genotype and treatment, were assayed. For all cases, $p < 0.05$ was considered significant.

3. Results

3.1. Syringin treatment mitigates the cognitive deficits of APP/PS1 mice

To assess whether syringin administration modulates cognition in APP/PS1 mice, we investigated the performance of mice in behavioural tasks reflecting learning and memory function. In the NORT, mice in both genotypes exhibited comparable exploration time and distance for the objects during initial environment habituation (*ps* > 0.05, Fig. 1A and B). The mice exhibited similar entries in the zone centre and edge of the open field (Fig. 1D and E). However, APP/PS1 mice exhibited poorer preferences for novelty in the short-term memory test phase (STM, 5-min retention interval) than age-matched WT mice ($F(1,38) = 37.810$,

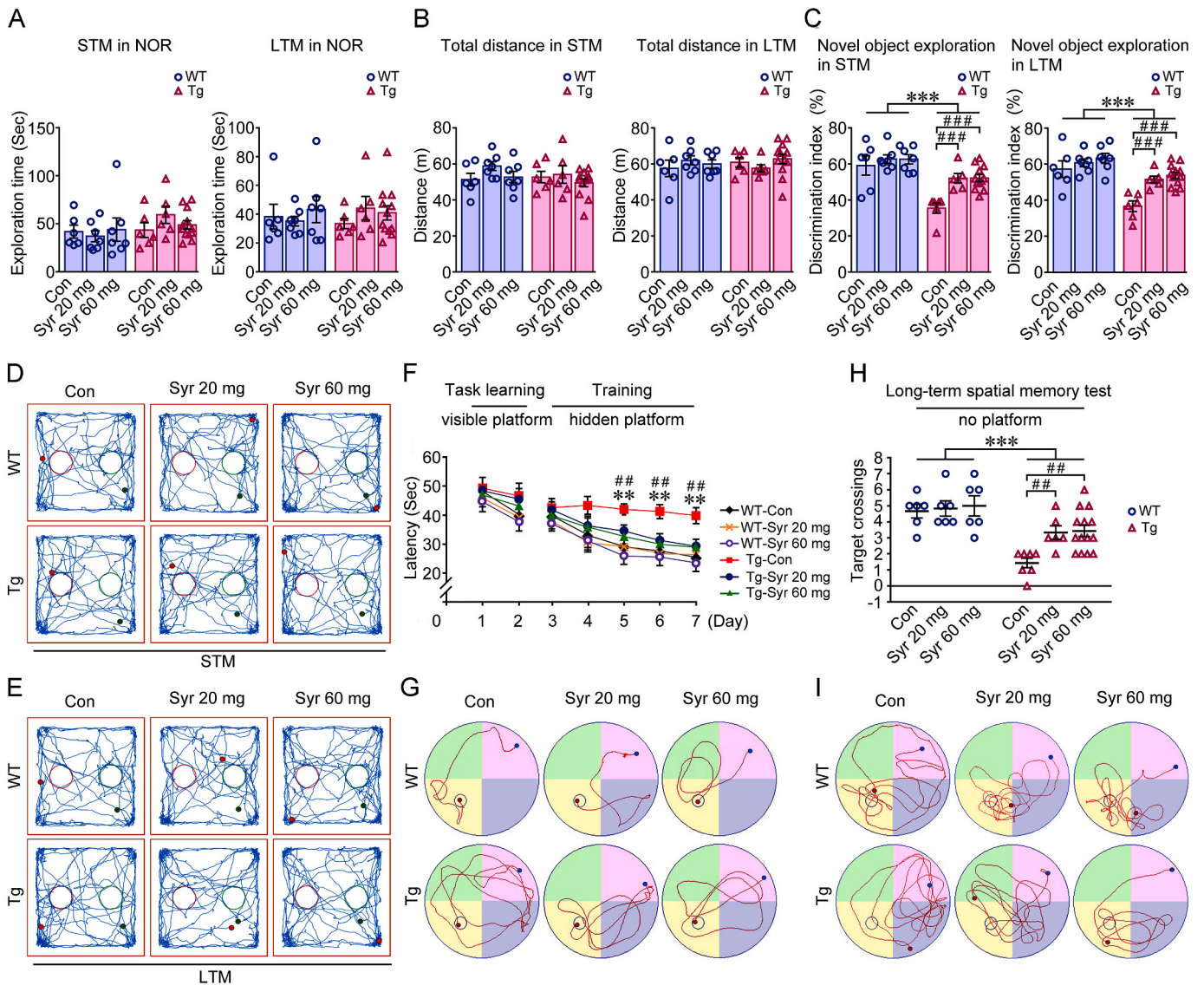

Fig. 1. Syringin treatment alleviates the cognitive impairment of APP/PS1 mice. Syringin (Syr) at dosages of 20 mg/kg or 60 mg/kg body weight was given by oral gavage to APP/PS1 transgenic (Tg) or age-matched wild-type (WT) C57BL/6 mice (starting from 4 months old) for 5 months. Mice treated with vehicle were used as the control group (Con). (**A-B**) A novel object recognition (NOR) test was performed to analyse the recognition memory of the mice. Short-term memory (STM) (5-min retention interval) and long-term memory (LTM) (24-h retention interval) analyses were presented. The mice exhibited comparable total exploration time and distance. (**C**) The discrimination index (calculated as the percentage of time spent exploring the new object/total exploration time) of Tg mice was significantly less than WT mice. Syr treatment ameliorates the discrimination index versus vehicle-treated group in the APP/PS1mice (***$p < 0.001$ relative to the WT group; $^{\#\#\#}p < 0.001$ relative to the vehicle group). Representative traces showing the exploration to the familiar (red circle) and the novel (green circle) object in the STM (**D**) and LTM (**E**) trial. Green dot indicates the location of the mouse when the test started, and the red dot represents the location of the animal when the test ended. (**F**) The Morris water maze (MWM) test was performed to assess the long-term and spatial memory of the mice. No significant differences in the escape latency were observed among the groups in the 2 days of the visible platform trial. During the following navigation test in which the mice searched for the hidden platform, Tg mice showed a longer escape latency than WT mice on the 5th, 6th and 7th day (**$p < 0.01$, WT versus Tg mice; $^{\#\#}p < 0.01$, Syr-treated Tg mice versus vehicle-treated Tg group). (**G**) Representative path graph showing the mice performance in hidden platform trial on the 7th day. (**H**) Quantification of probe trials on the 8th day (no platform) in the MWM test showed the number of times that the mice crossed through the location in which the platform had been previously placed. Tg mice exhibited fewer passing times than the WT mice. Syr treatment increased the number of times that the Tg mice passed across the location (***$p < 0.001$ relative to the WT group; $^{\#\#}p < 0.01$ relative to the vehicle group). (**I**) Representative path graph recording the performance of the mice in the probe trials (without platform) of the MWM test. Blue dot represents the location of the animal when the test started, and the red dot indicates the location of the mouse when the test ended. All data are presented as the mean ± S.E.M. Repeated measures ANOVA with *post hoc* Fisher's PLSD tests were applied to estimate the statistical significance. (For interpretation of the references to color in this figure legend, the reader is referred to the Web version of this article.)

$p < 0.001$, Fig. 1C and D). In the long-term memory test phase (LTM, 24 h retention interval), the exploration time of APP/PS1 mice on the unfamiliar object was less than that of WT mice ($F(1,38) = 35.210$, $p < 0.001$, Fig. 1C,E). In contrast, syringin-treated APP/PS1 mice exhibited significantly longer novel object exploration time than vehicle-treated APP/PS1 mice in both STM ($F(2,17) = 20.618$, $p < 0.001$, Fig. 1C–E) and LTM ($F(2,21) = 16.581$, $p < 0.001$, Fig. 1C–E) test phase, suggesting that their capacity to remember the familiar object were improved under syringin administration. No significant alteration of discrimination index was observed between syringin- and vehicle-treated WT mice in STM ($F(2,17) = 0.370$, $p > 0.05$) and LTM ($F(2,21) = 0.881$, $p > 0.05$) memory test phase. No genotype × syringin treatment interactions were observed in the NORT analyses ($ps > 0.05$).

Spatial learning and memory of the mice were evaluated using the

MWM test. During training with the visible platform, both genotypes of mice exhibited similar escape distances and latencies ($ps > 0.05$, Fig. 1F). All mice could swim in a coordinated way, and neither significant motivational nor significant motor defects were observed. In the hidden platform tests, the APP/PS1 mice presented impaired learning by longer escape distances and latencies relative to age-matched WT mice ($ps < 0.01$, Fig. 1F and G), and this deficit was alleviated by syringin administration ($ps < 0.01$, Fig. 1F and G). In the water maze probe trial, the APP/PS1 mice passed across the place where the original platform was located significantly fewer times than WT mice ($F(1,39) = 32.253$, $p < 0.001$, Fig. 1H and I). APP/PS1 mice in the syringin treatment group exhibited better memory retention than vehicle-treated APP/PS1 mice. The syringin-administered APP/PS1 mice crossed the original platform location more times than vehicle-treated APP/PS1 mice ($F(2,24) = 7.950$, $p < 0.01$, Fig. 1H and I). No genotype × syringin interaction was observed in the escape latency or probe trial ($ps > 0.05$). Syringin intervention on WT mice did not significantly affect their escape latency, although there was a trend towards a decrease ($ps > 0.05$, Fig. 1F and G), or the times of mice passing the platform location in the probe trial ($F(2,15) = 0.103$, $p = 0.902$, Fig. 1H and I).

3.2. Syringin treatment prevents the impairment of hippocampal synaptic plasticity in the brains of APP/PS1 mice

We examined hippocampal synaptic plasticity in APP/PS1 and age-matched WT mice. Acute hippocampal slices were prepared, and LTP in the CA1 region elicited by the stimulation of Schaffer collaterals was recorded. LTP deficits were observed in the APP/PS1 mice. As shown in Fig. 2A, there were significant differences in the basal synaptic transmission between APP/PS1 mice and age-matched WT mice ($ps < 0.01$). The calculation of the paired pulse ratio showed that the strength of presynaptic inputs in the hippocampus of APP/PS1 mice was weaker than that of the WT mice ($ps < 0.01$, Fig. 2B). Syringin treatment caused significant increases in the presynaptic release properties in the APP/PS1 mice ($ps < 0.01$, Fig. 2B). We calculated the minimum and maximum fEPSP slope at 100 μA and 350 μA, respectively. The minimum ($F(1,39) = 17.684$, $p < 0.001$, Fig. 2C) and maximum ($F(1,39) = 23.617$, $p < 0.001$, Fig. 2C) output in APP/PS1 mice were reduced compared with those of the WT group. However, syringin treatment led to an increase of APP/PS1 group in the minimum ($F(2,24) = 37.607$, $p < 0.001$) and maximum ($F(2,24) = 68.472$, $p < 0.001$) output relative to vehicle-administrated APP/PS1 mice (Fig. 2C). No statistical differences of minimum ($F(2,15) = 0.172$, $p > 0.05$) and maximum ($F(2,15) = 1.762$, $p > 0.05$) output were observed between Syr-with vehicle-treated WT group. No genotype × syringin interaction was observed in the basal synaptic transmission ($ps > 0.05$). In comparison with the typical LTP response induced by high-frequency stimulation in the hippocampus of WT mice, impaired LTP was observed in the APP/PS1 mouse brain. As shown in Fig. 2D and E, the degree of LTP in the APP/PS1 mice was prominently lower than that in the WT group. The LTP magnitude was significantly increased with syringin administration in the APP/PS1 mice relative to the magnitude in their vehicle-matched controls ($ps < 0.01$, Fig. 2D). No significant changes of hippocampal LTP magnitude were observed between Syr-with vehicle-treated WT group ($p > 0.05$, Fig. 2D). Synaptic protein levels were assayed by Western blot analyses. As shown in Fig. 2F, the protein expression of PSD-95, a postsynaptic density protein, were reduced in the hippocampus of APP/PS1 mice compared with those in the age-matched WT group ($F(1,30) = 134.341$, $p < 0.001$, Fig. 2F). The protein levels of synaptophysin (SYN), a specific marker for a presynaptic vesicle protein, exhibited a decrease in the APP/PS1 mouse brain in comparison with those in the WT controls ($F(1,30) = 46.833$, $p < 0.001$, Fig. 2F). Syringin administration mitigated the decreases in SYN ($F(2,15) = 12.495$, $p < 0.01$, Fig. 2F) and PSD-95 ($F(2,15) = 14.533$, $p < 0.001$, Fig. 2F) in the APP/PS1 mice. Meanwhile, syringin treatment caused significant increases in the protein expression of synaptic vesicles-related protein, synapsin-1, in both APP/PS1 ($F(2,15) = 84.563$, $p < 0.001$, Fig. 2F) and WT ($F(2,15) = 3.871$, $p < 0.05$, Fig. 2F) mice. No significant differences in the protein expression of SYN ($F(2,15) = 0.497$, $p > 0.05$, Fig. 2F) and PSD-95 ($F(2,15) = 2.886$, $p > 0.05$, Fig. 2F) were observed between the syringin- and vehicle-treated WT mice, although there was a trend towards an increase. Morphological assays of dendrites and spines showed dystrophy of neurites and decreases in dendrite areas ($F(1,42) = 87.795$, $p < 0.001$, Fig. 2G), spine areas ($F(1,42) = 88.441$, $p < 0.001$, Fig. 2G) and spine density ($F(1,42) = 19.932$, $p < 0.05$, Fig. 2G) in the APP/PS1 mouse brains compared with those in the WT group. In contrast, syringin treatment alleviated the loss of dendrite areas ($F(2,21) = 9.911$, $p < 0.01$), spine areas ($F(2,21) = 11.297$, $p < 0.001$) and spine density ($F(2,21) = 14.209$, $p < 0.001$) relative to vehicle treatment controls in the APP/PS1 mouse brains (Fig. 2G). No between-group alterations were detected in the dendrite areas ($F(2,21) = 0.893$, $p > 0.05$), spine areas ($F(2,21) = 0.361$, $p > 0.05$) or density ($F(2,21) = 0.453$, $p > 0.05$) between the syringin- and vehicle-treated groups in the WT mouse brains (Fig. 2G). No genotype × syringin interaction was observed in the effects on the synaptic protein levels ($ps > 0.05$, Fig. 2G).

3.3. Syringin administration alleviates the AD-like pathology and exhibits neuroprotective function in the brains of APP/PS1 mice

To evaluate the effects of Syringin on Aβ deposition in the APP/PS1 mice brains, Aβ levels were assayed. Human Aβ ELISA analysis revealed that soluble Aβ1-42 levels were significantly lower in the syringin-treated APP/PS1 mouse brains than those in the vehicle-treated group ($F(2,21) = 61.772$, $p < 0.001$, Fig. 3A). Syringin had similar effects on soluble Aβ1-40 contents ($F(2,21) = 8.862$, $p < 0.01$, Fig. 3A). The ratio of soluble Aβ42 to Aβ40 were significantly reduced ($F(2,21) = 3.593$, $p < 0.05$, Fig. 3A) in the syringin-treated APP/PS1 mouse brains relative to vehicle controls. So as the effects of syringin management on the insoluble Aβ1-40 ($F(2,21) = 5.603$, $p < 0.05$) and insoluble Aβ1-42 ($F(2,21) = 57.323$, $p < 0.001$) contents, and the insoluble Aβ42/Aβ40 ratio ($F(2,21) = 3.943$, $p < 0.05$, Fig. 3A) relative to the vehicle controls. To evaluate the effects of syringin on Aβ distribution and deposition in the brains of APP/PS1 mice, Aβ plaque was analysed by immunofluorescence labelling with the anti-pan-Aβ antibody. As shown in Fig. 3B, syringin-treated APP/PS1 mice exhibited significantly less amyloid deposition in the cortex and hippocampus than vehicle-treated APP/PS1 mice. We performed morphometry quantification of the Aβ plaque based on the diameter. Compared with the vehicle-treated APP/PS1 mice, the syringin-treated APP/PS1 mice exhibited fewer Aβ plaques with diameters greater than 50 μm in the cortex ($F(2,21) = 90.084$, $p < 0.001$, Fig. 3B) and hippocampus ($F(2,21) = 49.097$, $p < 0.001$, Fig. 3B). Furthermore, the numbers of Aβ plaques with dimeters at 25–50 μm of the Syr-treated mice were reduced in the cortex ($F(2,21) = 18.413$, $p < 0.001$, Fig. 3B) and hippocampus ($F(2,21) = 17.271$, $p < 0.001$, Fig. 3B) relative to those in the vehicle controls, respectively. There were no statistical differences in the numbers of small Aβ plaques (<25 μm) in the cortex ($F(2,21) = 2.372$, $p > 0.05$, Fig. 3B) and hippocampus ($F(2,21) = 3.476$, $p = 0.05$, Fig. 3B) among these three groups. Nissl stains were performed to assess the neuroprotective functions of syringin on the mouse brain. As shown in Fig. 3C, compared with syringin-treated APP/PS1 mice, vehicle-treated APP/PS1 mice exhibited significant nuclear breakdown and less intact Nissl substance in the hippocampus. Surviving neuronal cells in syringin-administrated group were increased than those of the vehicle controls in the CA1 ($F(2,21) = 48.124$, $p < 0.001$) and CA3 regions ($F(2,21) = 62.274$, $p < 0.001$). No difference was observed in the hippocampal Nissl staining between the different doses of syringin treatment ($ps > 0.05$, Fig. 3C). We estimated the effects of syringin on the cells apoptosis from the hippocampus using the Annexin V-FITC/PI staining by flow cytometry. As shown in Fig. 3D, the population of apoptotic cells from the hippocampus of syringin-administrated mice was significantly reduced with respect to that from the vehicle-treated APP/PS1 group. We then estimated the possible effects of

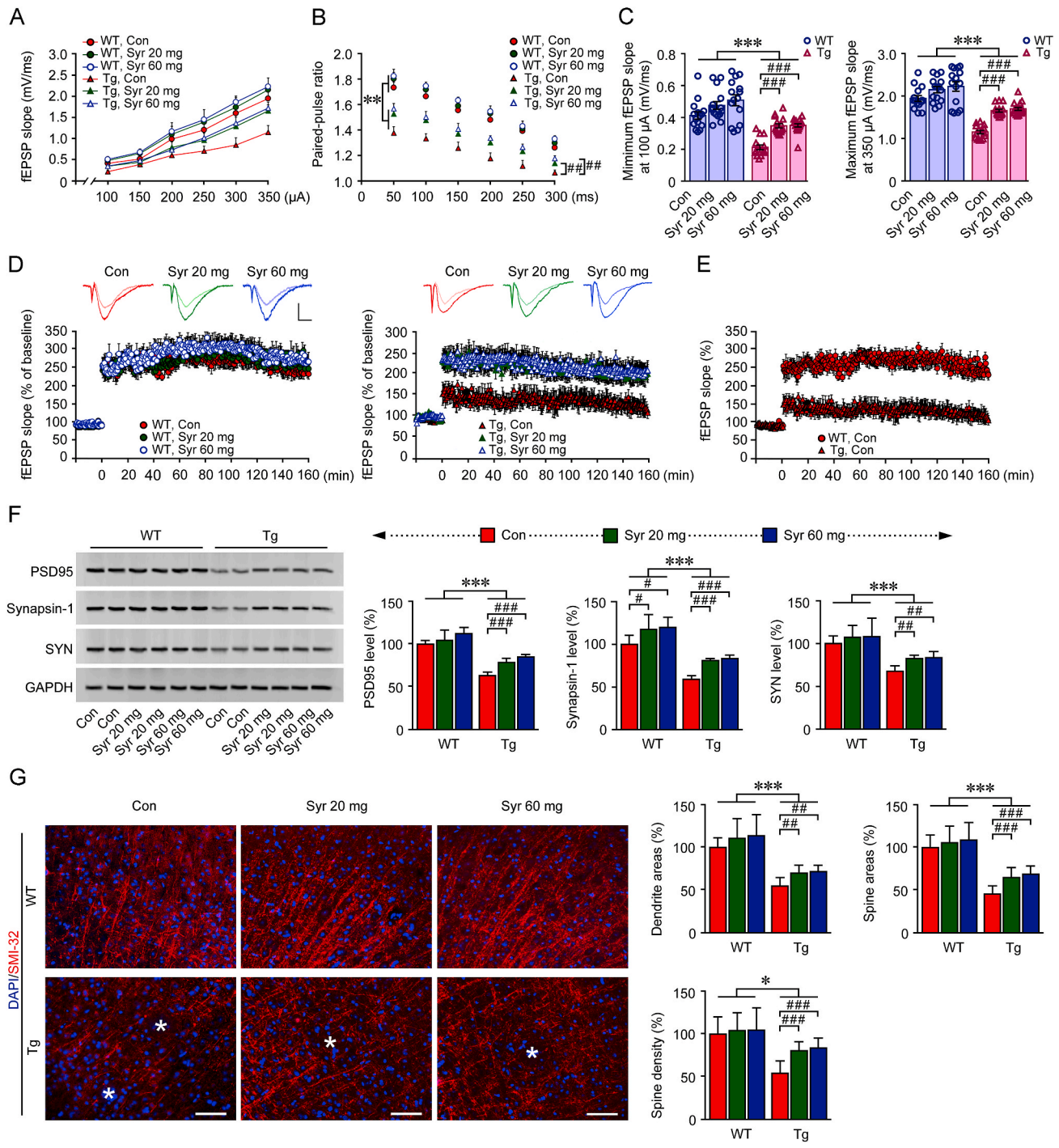

Fig. 2. Syringin administration ameliorates the hippocampal synaptic plasticity in the APP/PS1 mice. Brain tissues were collected from APP/PS1 transgenic (Tg) and age-matched wild-type (WT) C57BL/6 mice given syringin (Syr, 20 mg/kg or 60 mg/kg body weight) or vehicle (Con) by oral gavage. (**A**) Basal synaptic transmission was estimated using acute brain slices containing the hippocampus. Input/output curves were calculated according to the field excitatory postsynaptic potentials (fEPSPs) in the CA1 stratum radiatum. (**B**) Paired pulse ratio was recorded to assess the presynaptic function ($^{**}p < 0.01$, Tg versus WT group; $^{\#\#}p < 0.01$ Syr-treated Tg versus vehicle-treated Tg group). (**C**) Comparative analysis of the minimum (100 μA) and maximum (350 μA) output. (**D**) Shown are the time course of long-term potentiation (LTP) in Tg and WT CA1 pyramidal neurons after high-frequency stimuli (HFS). Top panels showing the sample traces before (light traces) and after (heavy traces) the HFS. Calibration bar: 1 mV/10 ms. (**E**) Comparison of the LTP magnitude between WT and Tg mice; replotted from (D). (**F**) Representative immunoblot images showing the protein expression of postsynaptic density 95 (PSD-95, postsynaptic components), synaptophysin (SYN, presynaptic components) and synapsin 1 (related to synaptic vesicles) in the hippocampus of the mouse brains ($^{***}p < 0.001$ relative to the WT group; $\#p < 0.05$, $\#\#p < 0.01$, $\#\#\#p < 0.001$ relative to the vehicle group). (**G**) The morphology of dendrites and spines (red) in the cortex of the mouse brains was displayed by immunostaining using an antibody against unphosphorylated neurofilament heavy chain (SMI-32). The nuclei (blue) were labelled with 4′,6-diamidino-2-phenylindole (DAPI). Asterisks indicate the losses of dendrites and spines in the APP/PS1 mice. Scale bars: 100 μm. Quantification showing the density and areas of the spines and the total dendrite areas ($^{*}p < 0.05$, $^{***}p < 0.001$ relative to the WT group; $\#\#p < 0.01$, $\#\#\#p < 0.001$ relative to the vehicle group). Two-way ANOVA with *post hoc* Fisher's PLSD tests were applied to assess the statistical significance. (For interpretation of the references to color in this figure legend, the reader is referred to the Web version of this article.)

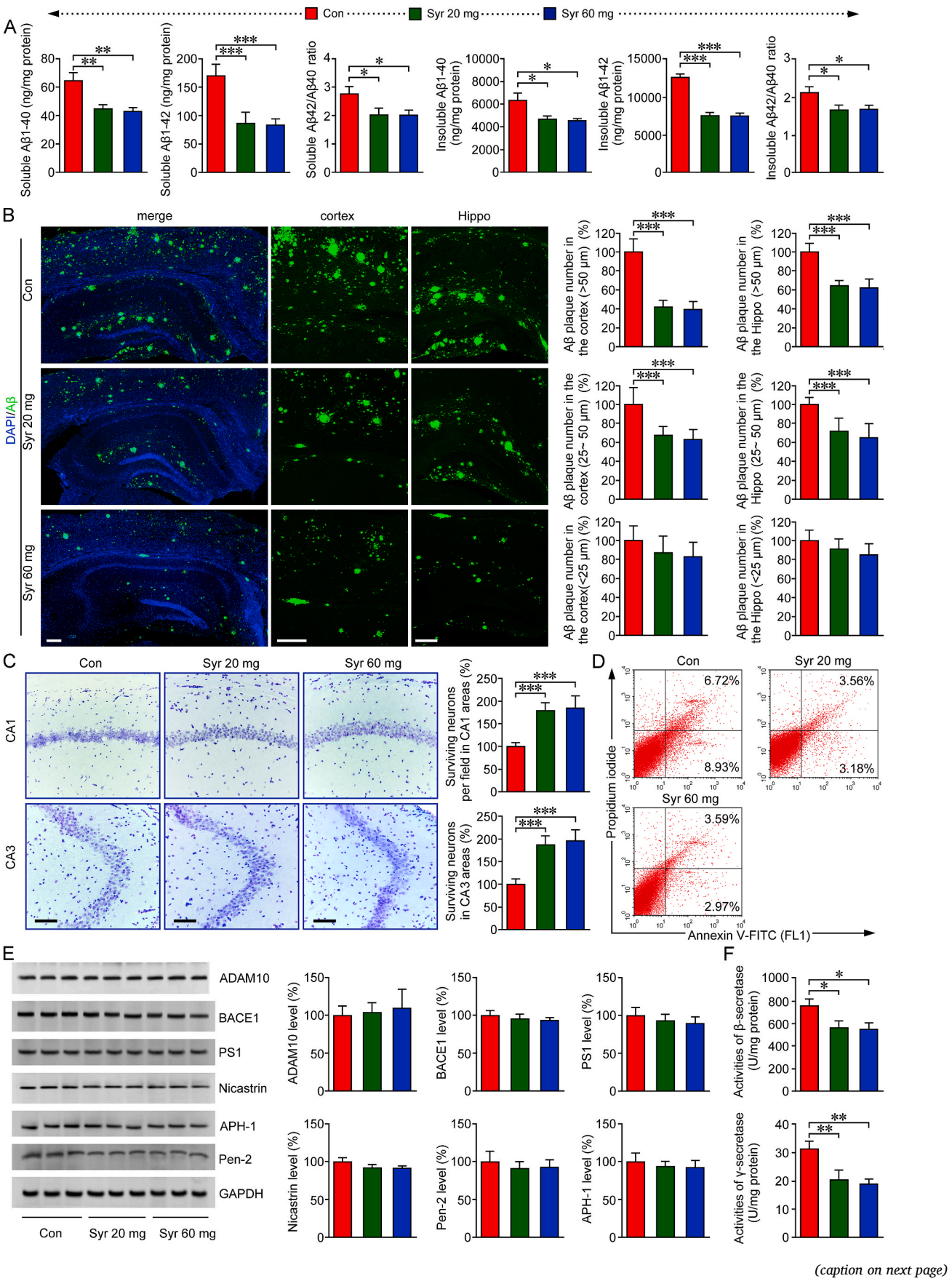

(caption on next page)

Fig. 3. Syringin management reduces Aβ accumulation and neuronal apoptosis in the brains of APP/PS1 mice. AD-related pathology in the mouse brains of APP/PS1 transgenic with syringin (Syr, 20 mg/kg or 60 mg/kg body weight) or vehicle treatment (Con) were detected. (**A**) Soluble and insoluble human Aβ1-42 and human Aβ1-40 levels were determined by ELISA. Quantification showing the ratio of Aβ1-42 to Aβ1-40. (**B**) Representative images of immunofluorescence staining with anti-Aβ antibody showing Aβ deposition (green) in the APP/PS1 mouse brain. DAPI was used to label nuclei (blue). High-magnification images of the cortex and hippocampus (Hippo) were depicted in the right panels. Scale bars: 200 μm. Relative percentages of Aβ plaques with various diameters were quantified. (**C**) Cresyl violet stains showing the Nissl body in the neuronal cells of the hippocampal CA1 and CA3 regions. Scale bars: 50 μm. The numbers of Nissl body indicate the surviving neurons. (**D**) Apoptosis levels of neuronal cells from the mouse brains were measured using Annexin V-FITC/PI staining by flow cytometry. (**E**) Representative Western blot images showing the protein expression of a disintegrin and metalloproteinase 10 (ADAM10), β-secretase 1 (BACE1) and γ-secretase, presenilin 1 (PS1), Nicastrin, APH-1 and Pen 2. (**F**) The β- and γ-secretase activities are shown. One-way ANOVA with *post hoc* Fisher's PLSD tests were adopted to estimate the statistical significance (*$p < 0.05$, **$p < 0.01$, ***$p < 0.001$ relative to the vehicle-treated controls). (For interpretation of the references to color in this figure legend, the reader is referred to the Web version of this article.)

syringin on cerebral amyloidosis attributed to the reduction in Aβ deposition in the syringin-treated APP/PS1 mouse brain. Western blot analyses were performed to detect the protein expressions of a disintegrin and metalloproteinase 10 (ADAM10), β-secretase 1 (BACE1) and γ-secretases (PS1, Nicastrin, APH-1 and Pen2). No between-group difference was observed in the protein expression of ADAM10, BACE1 or the γ-secretases, PS1, Nicastrin, APH-1, or Pen-2 (*ps* > 0.05, Fig. 3E), although there was a trend towards a decrease in the PS1 protein expressions in the syringin-treated mouse brains compared to that in the vehicle controls. The syringin-induced decline in β-secretase activities were significant ($F(2,21) = 3.798$, $p < 0.05$, Fig. 3F), and the effects of syringin treatment on γ-secretase activities were as well ($F(2,21) = 9.575$, $p < 0.01$, Fig. 3F).

3.4. Syringin administration upregulates iASPP and inhibits p53 DNA-binding activity without affecting p53 target gene transcription in the APP/PS1 mouse brain

The expression and activity of p53 are increased in AD brains [43]. It has been reported that p53 could transcriptionally activate pro-apoptotic genes or directly impair mitochondria function [44]. p53 apoptotic activities are tightly modulated by apoptosis-stimulating proteins of p53 (ASPP) family [14,15]. We explore whether syringin-induced amelioration of AD-related pathology and neuronal apoptosis is related to the modulation of p53. As shown in Fig. 4A, Western blot assays showed higher protein expressions of p53 in the nucleus ($F(1,30) = 25.090$, $p < 0.05$) and cytosol ($F(1,30) = 35.629$, $p < 0.05$) from the APP/PS1 mouse brains than those of age-matched WT mouse brains. Parallel to the increases in protein expressions, the mRNA levels of p53 were increased in the APP/PS1 mouse brains compared with those in the WT controls ($F(1,30) = 61.455$, $p < 0.05$, Fig. 4B). The DNA-binding activity of p53 was upregulated in the APP/PS1 mouse brain relative to that in the age-matched WT mice ($F(1,42) = 23.745$, $p < 0.05$, Fig. 4C). Syringin treatment reduced the protein expressions of p53 in the nuclei ($F(2,15) = 11.700$, $p < 0.01$, Fig. 4A) and cytoplasm ($F(2,15) = 9.222$, $p < 0.01$, Fig. 4A), and the p53 DAN-binding activity ($F(2,21) = 24.840$, $p < 0.001$, Fig. 4C) in the APP/PS1 mouse brains with respect to those of vehicle-treated APP/PS1 mice. The protein levels of cytosolic p53 were reduced in the WT mouse brains under syringin treatment relative to vehicle-treated WT controls ($F(2,15) = 6.022$, $p < 0.05$, Fig. 4A), the effects of syringin on the DNA-binding activities of p53 in the WT mouse brains were as well ($F(2,21) = 4.917$, $p < 0.05$, Fig. 4C). However, no obvious differences in the protein expressions of nuclear p53 were observed between syringin- and vehicle-treated WT mice ($F(2,15) = 1.631$, $p > 0.05$, Fig. 4A). Syringin treatment did not alter the mRNA levels of p53 in the WT mouse brains ($F(2,15) = 2.941$, $p > 0.05$, Fig. 4B).

We analysed the ASPP family members, iASPP, ASPP1 and ASPP2 in the APP/PS1 and age-matched WT mouse brain with or without syringin administration. The results of Western blot analyses revealed a marked decrease in iASPP protein expression in the nuclear fractions ($F(1,30) = 570.640$, $p < 0.001$, Fig. 4A) and cytoplasm ($F(1,30) = 86.859$, $p < 0.05$, Fig. 4A) of brain tissue from APP/PS1 mice compared to those in the age-matched WT group. The iASPP mRNA levels in the APP/PS1 mouse brains were lower than those from the WT mouse brains ($F(1,30) = 32.839$, $p < 0.05$, Fig. 4B). Syringin treatment led to an increase in iASPP protein expression from the cytoplasm of both WT ($F(2,15) = 4.681$, $p < 0.05$, Fig. 4B) and APP/PS1 ($F(2,15) = 20.622$, $p < 0.001$, Fig. 4A) mouse brains in comparison with those of their vehicle controls. Meanwhile, the protein expressions of nuclear iASPP ($F(2,15) = 12.672$, $p < 0.01$, Fig. 4B) and iASPP mRNA levels ($F(2,15) = 5.033$, $p < 0.05$, Fig. 4B) were increased in syringin-treated mouse brains relative to those of their vehicle controls in the APP/PS1. Syringin treatment did not significantly alter the protein levels of iASPP in the nucleus ($F(2,15) = 1.643$, $p > 0.05$, Fig. 4A) and iASPP mRNA levels ($F(2,15) = 3.343$, $p > 0.05$, Fig. 4B) in the WT mouse brains, a trend towards an increase. There were no significant differences in ASPP1 or ASPP2 protein expression between APP/PS1 and WT mouse brains (*ps* > 0.05, Fig. 4A). The mRNA levels of ASPP1 and ASPP2 in the APP/PS1 mouse brains were comparable to those in the WT mouse brains (*ps* > 0.05, Fig. 4B). Syringin treatment did not change the protein expression or the mRNA levels of ASPP1 in either WT or APP/PS1 mouse brains (*ps* > 0.05, Fig. 4B). The effects of syringin on ASPP2 mRNA levels were as well (*ps* > 0.05, Fig. 4B). To evaluate whether syringin-induced increases of iASPP could affect the iASPP-p53 or ASPPs-p53 interactions, we detected the iASPP-p53 and ASPPs-p53 complex by coimmunoprecipitation (Co-IP). As shown in Fig. 4D, the interaction of iASPP with p53 was less in the APP/PS1 mouse brains than that in the WT mouse brains ($F(1,30) = 228.549$, $p < 0.01$). No obvious differences in the ASPP1-p53 and ASPP2-p53 interactions were observed between the APP/PS1 and WT mice group (*ps* > 0.05, Fig. 4D). Syringin treatment caused an upregulation in the binding of iASPP to p53 in both WT ($F(2,15) = 23.013$, $p < 0.001$) and APP/PS1 mouse brains ($F(2,15) = 7.992$, $p < 0.01$) relative to their vehicle controls, without affecting the interactions of ASPPs-p53 (*ps* > 0.05). No genotype × syringin interaction was observed in the regulation of p53 activities and apoptosis-stimulating proteins of p53 (*ps* > 0.05). We performed a ChIP assay to assess the effects of syringin-induced alteration of iASPP on the known p53 target gene, Bax and PUMA, in the APP/PS1 mouse brain. As shown in Fig. 4E, the recruitment of p53 to PUMA ($F(1,30) = 698.342$, $p < 0.01$) and Bax ($F(1,30) = 470.564$, $p < 0.01$) were higher in the APP/PS1 mouse brains than those of their age-matched WT controls. Syringin treatment did not significantly change the transactivation of PUMA or Bax in both mouse genotypes in comparison with their vehicle controls (*ps* > 0.05). The results suggested that syringin-triggered increases of iASPP might not affect the transcriptional functions of p53.

3.5. Syringin treatment reduces oxidative stress in the brains of APP/PS1 mice

Considering the role of the aging-associated increase in oxidative stress in triggering enhanced Aβ plaque deposition [45] and apoptosis [46], we analysed the oxidative status in the APP/PS1 mice and age-matched WT mice under syringin or vehicle treatment. We first assessed the levels of 8-isoprostane, a biomarker for oxidative stress, in the blood serum of the mice. We observed that the 8-isoprostane levels were prominently higher in the plasma of APP/PS1 mice than that of the age-matched WT controls ($F(1,42) = 86.758$, $p < 0.05$, Fig. 5A). Syringin

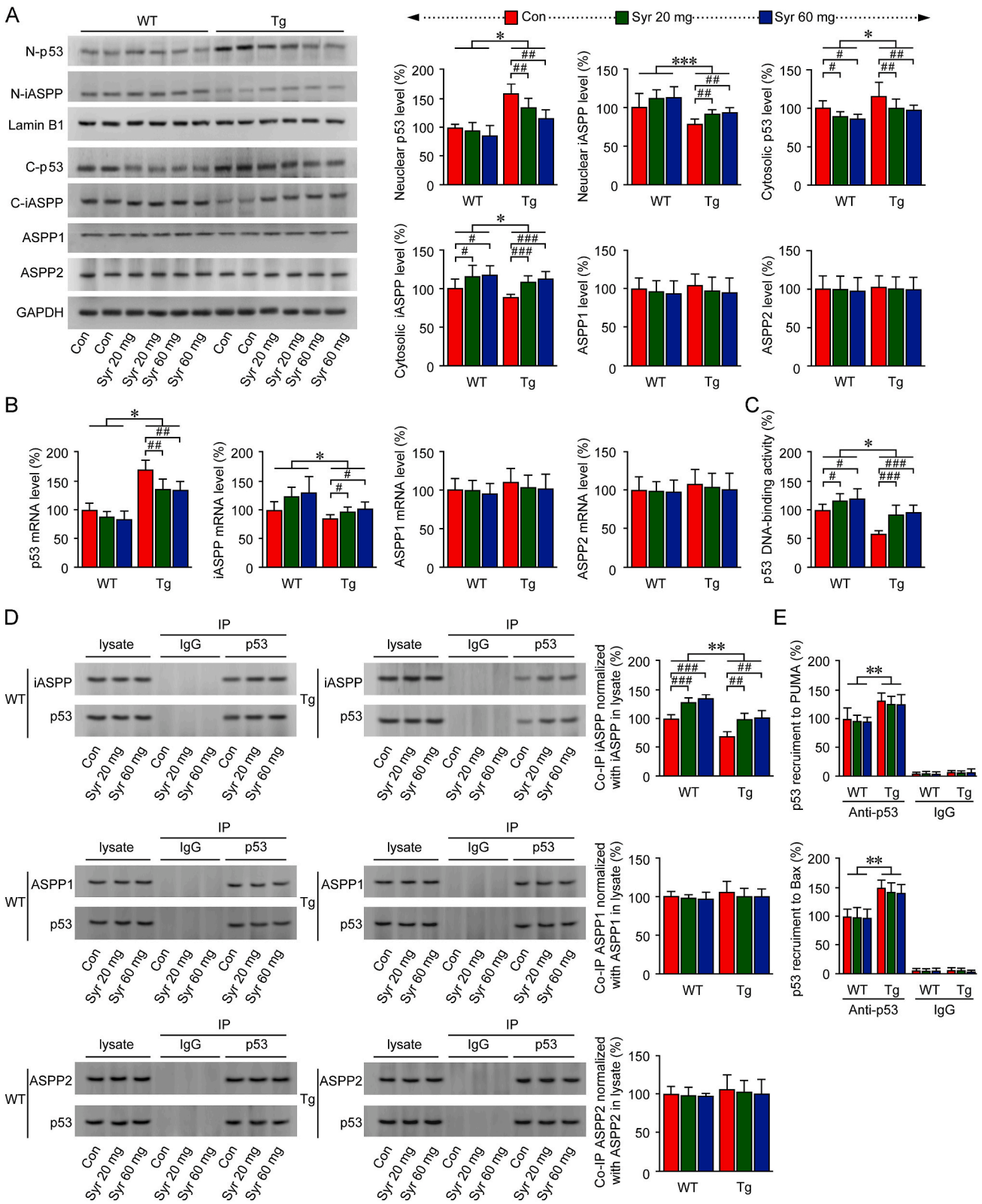

Fig. 4. Effects of syringin treatment on regulating p53 and the members of the apoptosis-stimulating protein of p53 (ASPP) family in the APP/PS1 mouse brains. The assessment of p53 in the nucleus (N-p53) and cytosol (C-p53), nuclear iASPP (N-iASP), cytosolic iASPP (C- iASPP), ASPP1 and ASPP2 in the mouse brains of APP/PS1 transgenic (Tg) and age-matched wild-type (WT) C57BL/6 mice given syringin (Syr, 20 mg/kg or 60 mg/kg body weight) or vehicle treatment (Con) were performed. Representative images of Western blot assays showing the protein levels (**A**). (**B**) mRNA levels of p53, iASPP, ASPP1 and ASPP2 were determined by real-time PCR. (**C**) Quantification showing the p53 DNA-binding activities. (**D**) The p53-iASPP interactions, the binding of p53 with ASPP1 and the p53-ASPP2 protein complex were measured by co-immunoprecipitation (CO-IP). (**E**) Chromatin immunoprecipitation (ChIP) analyses were performed to estimate p53-mediated gene transcription of PUMA and Bax. Two-way ANOVA with *post hoc* Fisher's PLSD tests ($^{*}p < 0.05$, $^{**}p < 0.01$, $^{***}p < 0.001$ relative to the WT group; $^{\#}p < 0.05$, $^{\#\#}p < 0.01$, $^{\#\#\#}p < 0.001$ relative to the vehicle-treated group).

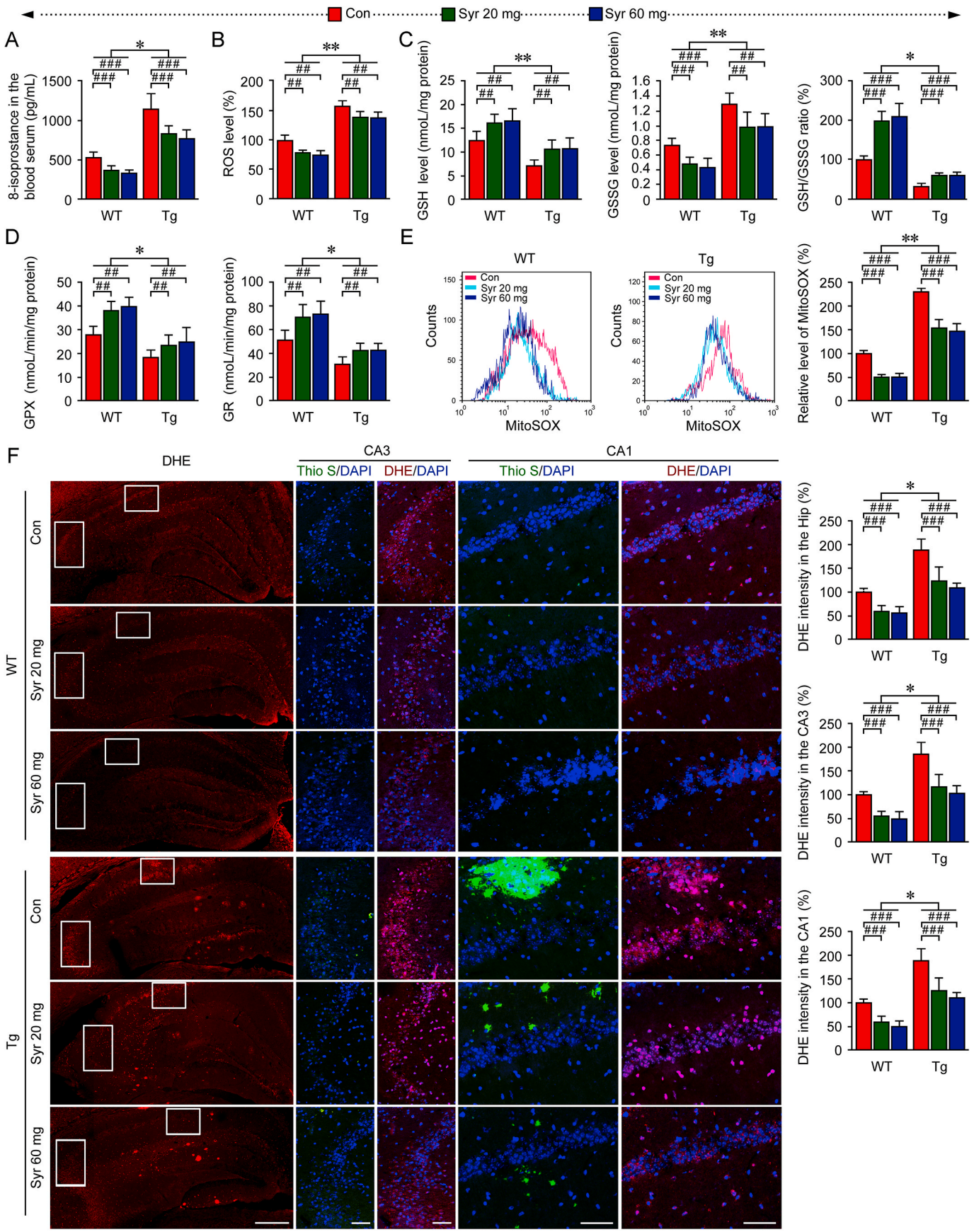

(caption on next page)

Fig. 5. Syringin administration amends the antioxidant defense in APP/PS1 mouse brains. (**A**) ELISA assays was performed to measure the levels of 8-isoprostane in the blood serum of APP/PS1 transgenic (Tg) and age-matched wild-type (WT) mice given syringin (20 mg/kg or 60 mg/kg body weight) or vehicle (Con) treatment. (**B**) ROS contents in the mouse brains were determined using CM-H2DCFDA fluorescence probe. (**C**) The contents of reduced glutathione (GSH) and oxidative glutathione (GSSG) in the brain tissues were assessed. Quantification showing the GSH/GSSG ratio. (**D**) The activities of glutathione peroxidase (GPX) and glutathione reductase (GR) were determined by colorimetric and ultraviolet colorimetric methods. (**E**) MitoSOX red assays by flow cytometry showing the levels of mitochondrial superoxide in the mouse brain. (**F**) Oxidized dihydroethidium (DHE) signal (red) showing the superoxide levels in the hippocampus of APP/PS1 and age-matched WT mice. Scale bars: 300 μm. High-magnification images of the CA3 and CA1 regions in the square boxes are depicted in the right panels. The high burden area of Aβ plques by Thioflavine (Thio S) labelled (green) also showing the significant positive staining of oxidized DHE. Scale bars: 60 μm. Two-way ANOVA with *post hoc* Fisher's PLSD tests (*$p < 0.05$, **$p < 0.01$ relative to the WT group; $^{\#\#}p < 0.01$, $^{\#\#\#}p < 0.001$ relative to the vehicle-treated group). (For interpretation of the references to color in this figure legend, the reader is referred to the Web version of this article.)

administration significantly reduced the 8-isoprostane contents in the plasma of both WT ($F(2,21) = 30.610$, $p < 0.001$, Fig. 5A) and APP/PS1 ($F(2,21) = 16.379$, $p < 0.001$, Fig. 5A) mice relative to their vehicle-treated control groups. We detected ROS levels by CM-H2DCFD probes and observed significantly higher ROS level in the brain tissue from APP/PS1 mice relative to that from the age-matched WT mice ($F(1, 42) = 416.848$, $p < 0.01$, Fig. 5B). The ROS contents of syringin-treated APP/PS1 mice were lower than those of the vehicle-treated APP/PS1 controls ($F(2,21) = 5.261$, $p < 0.01$, Fig. 5B). Syringin also reduced ROS production in the age-matched WT brains ($F(2,21) = 15.915$, $p < 0.01$, Fig. 5B). We then estimated the GSH and GSSG contents in the mouse brains. As shown in Fig. 5C, in comparison with age-matched WT controls, the APP/PS1 mice exhibited lower levels of GSH in the brains of APP/PS1 mice ($F(1,42) = 665.851$, $p < 0.01$) but significantly higher levels of GSSG ($F(1,42) = 172.944$, $p < 0.01$). Syringin treatment markedly increased the GSH contents in the brains of both WT ($F(2,21) = 7.208$, $p < 0.01$, Fig. 5C) and APP/PS1 mice ($F(2,21) = 10.599$, $p < 0.01$, Fig. 5C) relative to those of their vehicle-treated controls. Compared with the vehicle controls, syringin administration reduced the GSSG levels in both WT ($F(2,21) = 20.356$, $p < 0.001$, Fig. 5C) and APP/PS1 ($F(2,21) = 9.108$, $p < 0.01$, Fig. 5C) mouse brains. Accordingly, the GSH/GSSG ratio was lower in the APP/PS1 mice than in that of age-matched WT mice ($F(1,42) = 19.107$, $p < 0.05$, Fig. 5C). An increase in the GSH/GSSG ratio was present in both syringin-administrated WT ($F(2,21) = 106.791$, $p < 0.001$, Fig. 5C) and syringin-treated APP/PS1 ($F(2,21) = 109.684$, $p < 0.001$, Fig. 5C) mouse brains. A significant decline in the GPX ($F(1,42) = 55.074$, $p < 0.05$, Fig. 5D) and GR activities ($F(1,42) = 75.412$, $p < 0.05$, Fig. 5D) was exhibited in the APP/PS1 mouse brains compared with those in the age-matched WT mouse brains. Syringin treatment enhanced the GPX and GR activities in both the WT and APP/PS1 mouse brains (*ps* < 0.01, Fig. 5D). Mitochondrial superoxide measurements by flow cytometry analyses with MitoSOX Red staining showed that the levels of mitochondrial superoxide anion in the APP/PS1 mouse brain were higher than those in the age-matched WT group ($F(1,42) = 121.385$, $p < 0.01$, Fig. 5E). Compared to vehicle treatment, syringin intervention markedly reduced the superoxide anion levels in the brains of WT ($F(2,21) = 70.453$, $p < 0.001$, Fig. 5E) and APP/PS1 ($F(2,21) = 31.613$, $p < 0.001$, Fig. 5E) mice. Consistent with MitoSOX results, morphological assays of endogenous superoxide levels with DHE staining revealed marked increases in the hippocampus of APP/PS1 mouse brains relative to those in their age-matched WT controls ($F(1,30) = 48.331$, $p < 0.05$, Fig. 5F). Double labelling with Thioflavine S (Thio S) and DHE indicated that the oxidized DHE fluorescence signal appeared to be more concentrated in the cell body and nuclei around the Aβ plaques regions in the hippocampal slices of APP/PS1 mice than those of the age-matched WT controls (Fig. 5F). In comparison with the WT mice, the superoxide dye were more greater in the hippocampal CA1 ($F(1,30) = 58.525$, $p < 0.05$, Fig. 5F) and CA3 ($F(1,30) = 48.331$, $p < 0.05$, Fig. 5F) areas of the APP/PS1 mouse brains. Whereas, striking decline of oxidized DHE were observed in entire hippocampus ($F(2,15) = 22.907$, $p < 0.001$, Fig. 5F), the CA3 ($F(2,15) = 22.134$, $p < 0.001$) and CA1 ($F(2,15) = 22.898$, $p < 0.001$) regions from Syr-administrated APP/PS1 mice compared with vehicle-treated APP/PS1 controls. The effects of Syr on superoxide contents in the age-matched WT mice were as well (*ps* < 0.001, Fig. 5F).

3.6. Syringin treatment increases the interaction of iASPP and Keap1 and stabilizes Nrf2 levels in the APP/PS1 mouse brain

Nrf2 is one of the most important endogenous regulators protecting cells against oxidative stress [9,47]. Nrf2 nuclear translocation is required to drive the transcription of antioxidative and cellular defence targets [8]. Nuclear Nrf2 protein expression has been reported to be significantly reduced in the hippocampal neurons of AD postmortem tissues [10]. IASPP competes with Nrf2 for binding with Keap1 and facilitates Nrf2 nuclear translocation in cancer cells [24]. To investigate whether syringin-induced upregulation of antioxidant defense in the APP/PS1 mouse brain is involved in the modulation of iASPP and Nrf2, we detected Nrf2 protein levels in the APP/PS1 and age-matched WT mouse brains. A band of approximately at ~110-95 kDa was observed using a rabbit anti-Nrf2 antibody, indicating that it was not a degraded Nrf2 [48]. As shown in Fig. 6A, the protein expressions of Nrf2 were lower in the nucleus ($F(1,30) = 584.881$, $p < 0.01$) and cytosol ($F(1,30) = 55.041$, $p < 0.05$) from the APP/PS1 mouse brains than those of the WT controls. The Nrf2 mRNA levels ($F(1,30) = 160.819$, $p < 0.01$, Fig. 6B) and DNA-binding activities ($F(1,30) = 537.940$, $p < 0.01$, Fig. 6C) were lower in the APP/PS1 mouse brains than in the age-matched WT group. Syringin treatment increased the protein expressions of nuclear Nrf2 in the APP/PS1 mouse brains relative to vehicle-treated APP/PS1 controls ($F(2,15) = 7.283$, $p < 0.01$, Fig. 6A). So as the effects of syringin on the protein levels of cytosolic Nrf2 in the APP/PS1 mouse brains ($F(2,15) = 7.082$, $p < 0.01$, Fig. 6A). Syringin administration enhanced the Nrf2 mRNA levels (*ps* < 0.001, Fig. 6C) and Nrf2 DNA-binding activities (*ps* < 0.001, Fig. 6C) in both APP/PS1 and WT mouse brains. We detected the interaction of iASPP with Keap1. Co-IP assays showed that the binding of iASPP to Keap1 was lower in the APP/PS1 mouse brain than that of the age-matched WT group ($F(1,30) = 216.759$, $p < 0.01$, Fig. 6D). Compared with vehicle-treated APP/PS1 mice, syringin-treated APP/PS1 mice exhibited an increase in the interaction of Keap1 with iASPP in the mouse brains ($F(2,15) = 11.199$, $p < 0.01$, Fig. 6D). Syringin similarly affected iASPP-Keap1 complex formation in the WT mouse brains as well ($F(2,15) = 11.303$, $p < 0.01$, Fig. 6D). Morphological stains with anti-iASPP antibody showed that the iASPP activity products were mainly located in the neuronal cytoplasm and nuclei (Fig. 6E). Co-staining with anti-iASPP antibody and Thio S showed that immunoreactivities of iASPP in the neurons were significantly less, especially around the Aβ plaque-related areas in the hippocampus of the APP/PS1 mouse brains (Fig. 6E). In contrast, the protein expressions of iASPP from syringin-treated APP/PS1 mice brains were markedly increased in the Aβ-related areas than those of vehicle-administrated APP/PS1 group (Fig. 6E). The morphological assays of Nrf2 distribution and expression revealed that the nuclear Nrf2 immunoreactivities were reduced in the hippocampal CA1 ($F(1,30) = 116.915$, $p < 0.01$, Fig. 6F) and CA3 regions ($F(1,30) = 245.415$, $p < 0.01$, Fig. 6F) from the APP/PS1 mice than those of age-matched WT controls. Syringin treatment facilitated Nrf2 nuclear translocation in both WT and APP/PS1 mice compared to their vehicle controls (*ps* < 0.01, Fig. 6F).

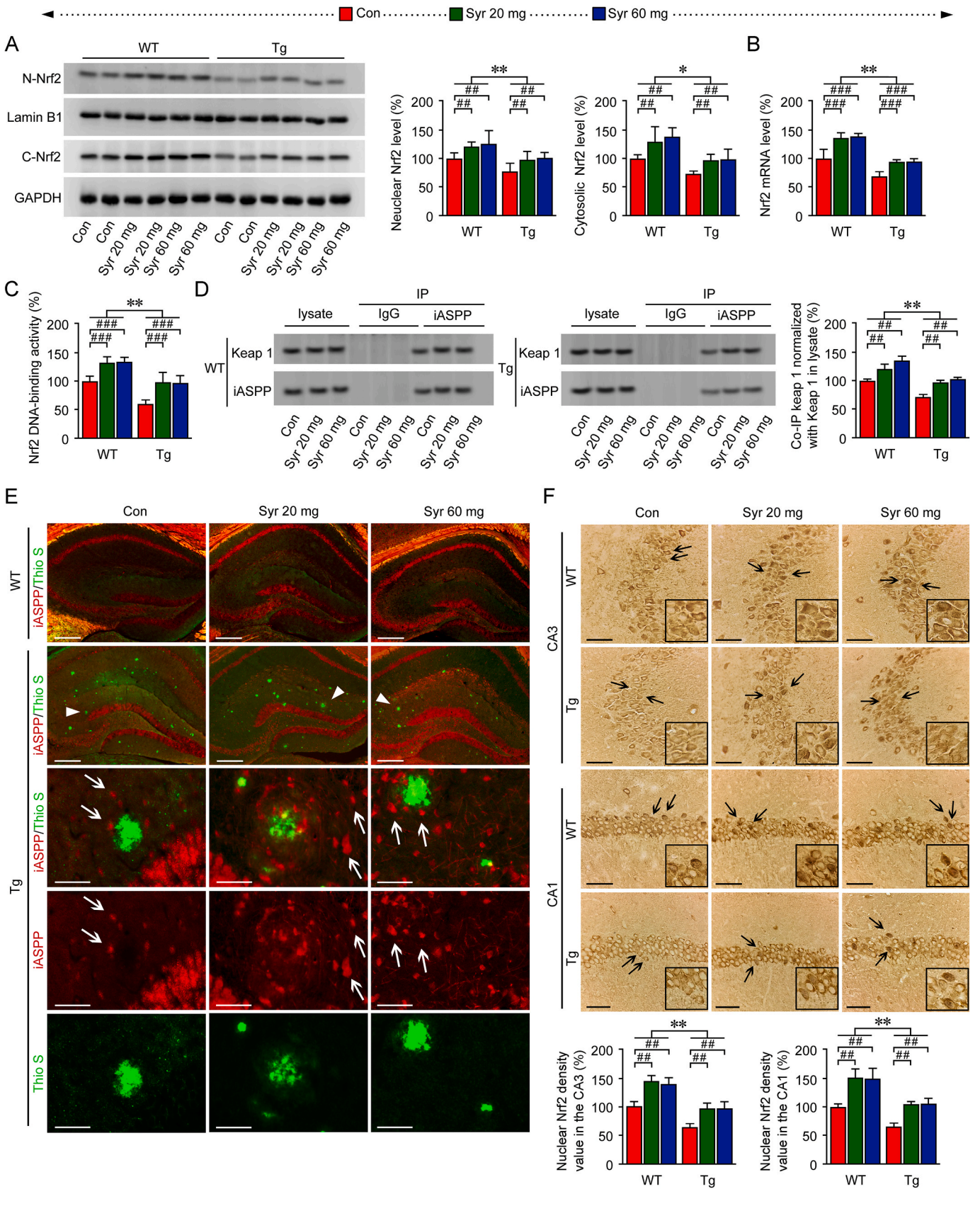

(caption on next page)

Fig. 6. Syringin management enhances the cytosolic iASPP-Keap1 interaction and the nuclear Nrf2 DNA-binding activity in the APP/PS1 mouse brain. (**A**) Western blot assays showing the protein expression of Nrf2 in the cytosol and nuclei of the brains in the APP/PS1 transgenic (Tg) and age-matched wild-type (WT) mice given syringin (20 mg/kg or 60 mg/kg body weight) or vehicle (Con) treatment. (**B**) mRNA levels of Nrf2 were examined by real-time PCR. (**C**) DNA-binding activities of Nrf2 were determined by ELISA assays. (**D**) The binding of Keap1 with iASPP was assessed by co-immunoprecipitation (Co-IP) assays. (**E**) Representative immunofluorescence images of iASPP (red) and Thioflavine (Thio S, green) labelling in the hippocampal sections of APP/PS1 and age-matched WT mouse brains. White arrows indicate the iASPP-immunoreactive cells around the Thio S-positive plaques. Scale bars: 200 μm. High-magnification images (the bottom three panels) show the localization of iASPP (indicated by white arrowheads) and Aβ-containing plaques. Scale bar = 60 μm. (**F**) Immunostaining with anti-Nrf2 antibody showing the cytosolic and nuclear localization of Nrf2 in the CA3 and CA1 regions of the hippocampus. Black arrowheads indicate the representative Nrf2-immunoreactive stains in the neuronal nuclei. Scale bars: 60 μm. Square boxes showing the high magnification. Two-way ANOVA with *post hoc* Fisher's PLSD tests (*$p < 0.05$, **$p < 0.01$ relative to the WT group; ##$p < 0.01$, ###$p < 0.001$ relative to the vehicle-treated group). (For interpretation of the references to color in this figure legend, the reader is referred to the Web version of this article.)

3.7. Syringin induces enhancement of antioxidant defense via the iASPP-Nrf2 axis

A previous study demonstrated that iASPP overexpression could facilitate Nrf2 accumulation and increase antioxidative functions in cancer cells [24]. Considering some common molecular mechanisms but inverse relationships underlying the onset and development of cancer and neurodegenerative diseases [49], we examined whether syringin-induced iASPP upregulation is involved in regulating the Nrf2 signalling cascade in AD model cells *in vitro*. To assess the protective effects of syringin under conditions similar to oxidative stress in AD-related pathology, N2a cells or N2a cells overexpressing human β-amyloid precursor protein Swedish mutation (APPswe) were treated with 50 μM H_2O_2, or pre-treated with 1-mM of syringin for 6 h and subsequently exposed to 50 μM H_2O_2 for 24 h. CM-H_2DCFDA probe labelling revealed that H_2O_2 treatment caused a marked increase in ROS production in both N2a and APPswe cells compared with vehicle controls (*ps* < 0.01, Fig. 7A). The ROS levels in H_2O_2-treated APPswe cells were higher than those of H_2O_2-treated N2a cells ($p < 0.05$, Fig. 7A). In contrast, syringin treatment alleviated the H_2O_2-induced increase in ROS in N2a cells ($p < 0.01$ Fig. 7A) and APPswe cells ($p < 0.01$, Fig. 7A). PI uptake analysis by flow cytometry revealed that chronic H_2O_2 treatment significantly reduced the portion of S-phase cells, but triggered more cells arrested in the G0/G1 phase in both APPswe and N2a cells relative to vehicle controls (Fig. 7B). The proportion of S-phase cells of the APPswe group in the presence of H_2O_2 was less than that of N2a cells under H_2O_2 treatment, indicating the vulnerable of APPswe cells to H_2O_2-induced cell cycle delay and DNA damage. Syringin treatment significantly prevented the H_2O_2-induced drop in the proportion of S-phase cells in both N2a cells and APPswe cells (Fig. 7B), suggesting syringin-mediated cells repair for the initial damage. Meanwhile, as shown in Fig. 7C, the population of H_2O_2-triggered apoptotic cells in APPswe cells was markedly higher than that of N2a cells. Syringin treatment significantly reduced H_2O_2-induced apoptosis in both N2a and APPswe cells. We then assessed the effects of oxidative stress on Aβ production. As shown in Fig. 7D, syringin treatment significantly inhibited H_2O_2-induced increases of Aβ1-40 and Aβ1-42 secretion in both N2a and APPswe cells (*ps* < 0.01).

Considering our present results showing syringin treatment-induced increases in iASPP expression and the stabilization of Nrf2 in the brains of APP/PS1 mice, we examined the modulatory effects of syringin on the iASPP/Nrf2 signal axis in N2a and APPswe cells *in vitro*. As shown in Fig. 7E, chronic H_2O_2-induced decreases in the protein expressions of cytosolic and nuclear iASPP were worsen in the APPswe cells than those in the N2a cells ($p < 0.01$), similar to the Nrf2 protein levels ($p < 0.01$, Fig. 7E), Nrf2 mRNA levels ($p < 0.01$, Fig. 7F) and Nrf2 DNA-binding activity ($p < 0.01$, Fig. 7G). Syringin treatment mitigated the chronic H_2O_2-triggered decline of iASPP and Nrf2 protein expressions in both cytosol and nucleus (*ps* < 0.01, Fig. 7E), and the Syringin-mediated effects on Nrf2 mRNA levels ($p < 0.01$, Fig. 7F) and DNA-binding activity of Nrf2 ($p < 0.01$, Fig. 7G) were as well. Chronic H_2O_2 treatment reduced the Keap1-iASPP interaction to a greater extent in the APPswe cells than in the N2a cells ($p < 0.01$, Fig. 7H). The binding of Keap1-iASPP was greater in H_2O_2-primed APPswe cells in the presence of syringin treatment than that in H_2O_2-treated APPswe cells in the absence of syringin ($p < 0.01$, Fig. 7H). An enhancement of the Keap1-iASPP interaction was also observed in H_2O_2-treated N2a cells given syringin treatment relative to the H_2O_2-primed N2a cell without syringin management ($p < 0.01$, Fig. 7H). We further verified that syringin triggered the upregulation of Nrf2, thereby protecting cells against oxidative stress *via* the modulation of iASPP. As shown in Fig. 7I, siRNA-induced inhibition of iASPP reduced the syringin-mediated increase in cytoplasmic and nuclear Nrf2 levels ($p < 0.01$, Fig. 7I) and partly abrogated the syringin-caused decreases in ROS in both N2a and APPswe cells ($p < 0.01$, Fig. 7J). Importantly, as shown in Fig. 7k and Supplementary 1 Fig. S1, lentiviral gene transfer (LV-iASPP)-triggered iASPP overexpression or syringin treatment could lead to the increases of protein expression (*ps* < 0.01, Fig. 7K) and mRNA levels (*ps* < 0.01, Supplementary Fig. S1) of NQO1 and γGCL-C, suggesting the transcription activation of Nrf2 downstream genes. However, Nrf2 siRNA or Nrf2 inhibitor, trigonelline, markedly abrogated the effects above (*ps* < 0.01). Our result suggests that syringin-induced upregulation of iASPP enhances antioxidant defense *via* the iASPP-Nrf2 axis. Computational docking of the molecular structure of syringin and iASPP showed that the binding affinity of iASPP on syringin was strong (−23.02 kJ/mol). Syringin forms hydrogen bonds with iASPP by Asparagine 687 (Asn687), Aspartic acid 768 (Asp768) and Asn813, respectively. The interaction between syringin and iASPP forms a binding pocket (Supplementary Fig. S2).

4. Discussion

Age-related oxidative imbalance is thought to be a prominent manifestation related to neuronal cell damage in the brain [50]. Chronic exposure to ROS is closely related to brain senescence and neurodegenerative diseases. Antioxidants are recognized to have great applicable potential for the management of neurodegenerative diseases [51]. Natural products, such as polyphenol compounds extracted from plants and herbs, has attracted attention because of their antioxidant properties [52]. Neuronal cells in the nervous system are highly sensitive to oxidative stress because of their higher dependence on oxidative phosphorylation for large metabolism-demanding processes than other cell types. Oxidative stress is an important pathogenic manifestation of AD that may contribute to synaptic dysfunction, which precedes Aβ accumulation and neurofibrillary tangle formation [53,54]. Antioxidant administration has been observed to be able to reduce oxidative stress and inhibit Aβ production *in vitro* [55]. Antioxidant treatment has been shown to improve performance on cognitive tests in AD animal models [56,57]. In an early intervention with antioxidants in mild to moderate AD patients, the patients who received treatment with the antioxidant colostrinin exhibited improved cognitive functions [58]. It is considered that restoring redox homeostasis is a potential protective strategy against brain ageing and neurodegenerative disease [59]. In the present study, we showed that the increase in oxidative stress in the APP/PS1 mouse brain was directly related to synaptic deficiency and cognitive impairment. Syringin was able to mitigate the oxidative-redox imbalances in the brains of APP/PS1 mice. Syringin treatment downregulated the activities of β- and γ-secretases and alleviated Aβ accumulation in the

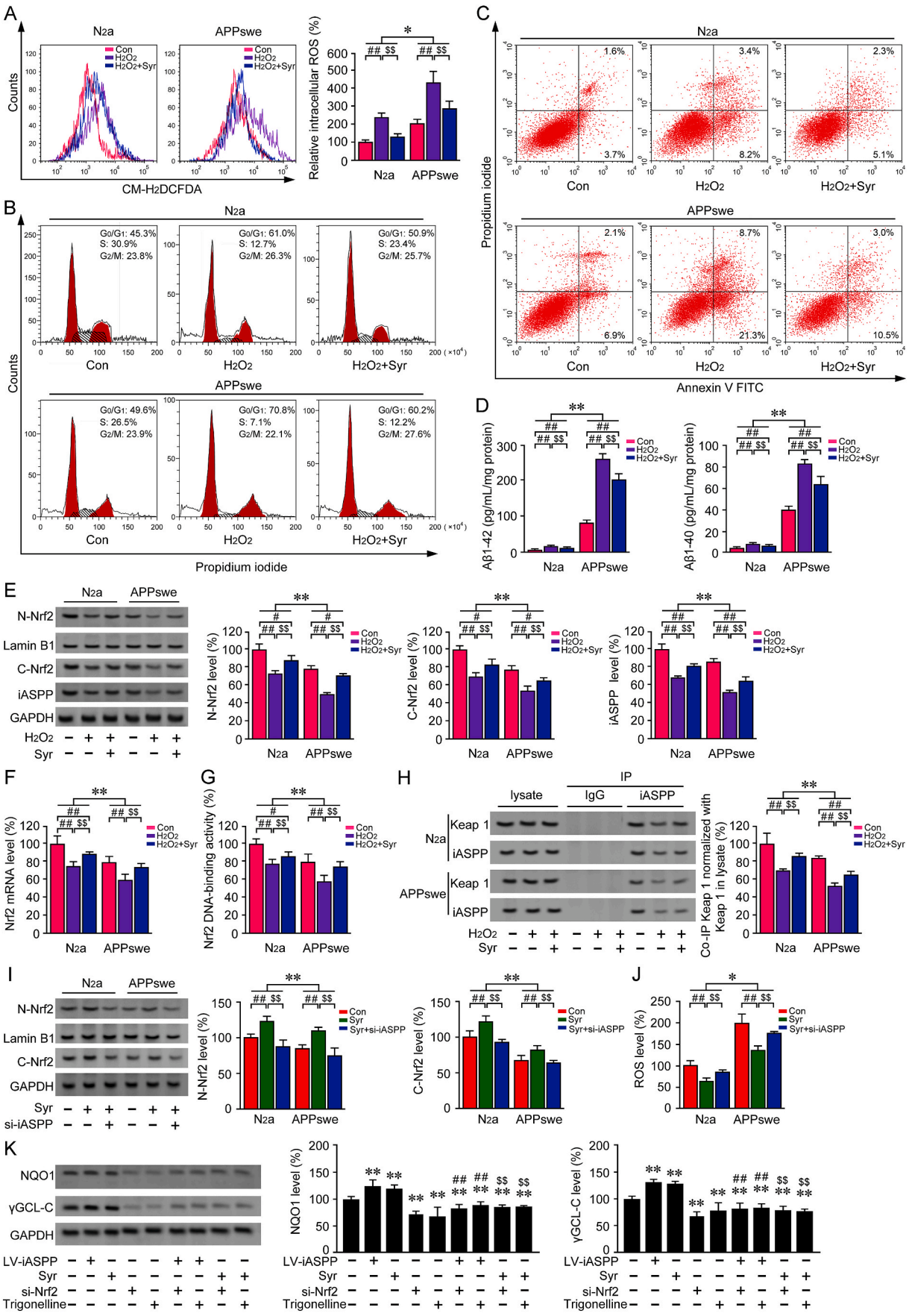

(caption on next page)

Fig. 7. IASPP increases mediated by syringin exert antioxidant activity and reduce apoptosis by stabilizing Nrf2. (**A**) ROS contents are significantly increased under H_2O_2 (50 μM, 24 h) treatment in N2a cells or N2a cells transfected with the human beta-amyloid precursor protein Swedish mutation (APPswe). N2a and APPswe cells with vehicle treatment were used as controls (Con). CM-H2DCFDA staining by flow cytometry assays showing that the ROS levels are markedly reduced under incubating with 1-mM of syringin (Syr) for 6 h followed by 50 μM H_2O_2 addition and up to 24 h in both N2a and APPsw cells. (**B**) Cell cycle of N2a and APPswe cells were evaluated. Quantification showing the propidium iodide (PI) uptake of cells. (**C**) Annexin V-FITC/PI staining showing the protective effects of syringin against H_2O_2-induced apoptosis in N2a and APPswe cells. (**D**) Soluble Aβ1-40 and Aβ1-42 levels secreted by the cells were measured by ELISA. (**E**) Representative Western blot images showing the protein expression of iASPP and Nrf2 in the nucleus (N-Nrf2) and the cytosol (C-Nrf2). (**F**) mRNA levels of Nrf2 are shown. (**G**) Nrf2 DNA-binding activity in the N2a and APPswe cells was measured. (**H**) The iASPP-Keap1 interactions in the N2a and APPswe cells were determined by Co-immunoprecipitation (Co-IP). The small interfering RNA (siRNA)-mediated inhibition of iASPP (si-iASPP, 50 nM) abolished syringin-triggered increases of Nrf2 levels in the cytoplasm and nuclei (**I**) and abrogated the syringin-induced ROS reduction (**J**) in the N2a and APPswe cells. (**K**) Western blot analysis showed that upregulation of NQO1 and γGCL-C triggered by iASPP lentiviral gene transfer (LV-iASPP) or Syr treatment were blocked by transfected with 60 nM of Nrf2 siRNA (si-Nrf2) or Nrf2 inhibitor, trigonelline (0.5 μM, 24h), in the APPswe cells. Statistical significance: $^{*}p < 0.05$, $^{**}p < 0.01$ relative to N2a controls; $^{\#\#}p < 0.01$ relative to the vehicle-treated group; $^{\$\$}p < 0.01$ relative to H_2O_2 treatment group. Data were analysed with multivariate ANOVA with *post hoc* Fisher's PLSD tests (A–H). $^{*}p < 0.05$, $^{**}p < 0.01$ relative to N2a controls; $^{\#\#}p < 0.01$ relative to the vehicle-treated group; $^{\$\$}p < 0.01$ relative to Syr treatment group. Data were analysed with multivariate ANOVA with *post hoc* Fisher's PLSD tests (I–J); $^{**}p < 0.01$ compared with the vehicle-treated group; $^{\#\#}p < 0.01$ compared with LV-iASPP management cells; $^{\$\$}p < 0.01$ relative to Syr-treated group. Data were analysed with one-way ANOVA with *post hoc* Fisher's PLSD tests (K). Values are represented at least three independent experiments.

APP/PS1 mouse brain, without altering the protein expressions of ADAM10, BACE1, PS1, APH-1, Nicastrin, and Pen-2. Our findings suggested that syringin-induced upregulation of antioxidant defense might exert critical roles in mitigating AD-related pathology.

An endogenous defence against oxidative stress is the activation of the Nrf2 signalling pathway [60]. Under physiological conditions, Nrf2 interacts with the cytoplasmic protein Keap1 [61] and is degraded [7]. Nrf2 is detached from Keap1 in response to stress stimuli and is translocated to the nucleus, potentially driving transcriptional activation of its target genes through acting on AREs, thereby exerting a cytoprotective response [5]. It has been reported that Nrf2 protein expression is abundant in the nuclei of neurons from normal human post-mortem brain [10]. Ramsey and colleagues revealed significant decreases of Nrf2 in human autopsy brain tissues of AD cases by immunoblotting assays. Nrf2 presented weakly expression in the nuclei of neurons in the hippocampus and frontal cortex of AD brain [10]. Nrf2 content has been reported to decline with age [62], and the Nrf2-mediated antioxidative response is lost in old rats [63]. Nrf2 deficiency makes neurons vulnerable to toxic stimuli *in vitro* [64]. Oxidative stress and neuroinflammation along with hyperphosphorylated tau and Aβ oligomer were significantly increased in the brains of AD model mice with Nrf2 knockout [65]. Upregulating Nrf2 signalling by stereotactic injection with lentiviral-Nrf2 to the hippocampal tissue of the APP/PS1 mouse brain alleviated the learning deficiency of the mice [12]. We previously observed that increasing Nrf2 expression enhanced CD36 expression and facilitated Aβ clearance [7]. In the present study, immunofluorescence labelling and immunohistochemistry staining respectively showed syringin-mediated increases of iASPP and nuclear translocation of Nrf2 in the hippocampal neurons of the mouse brains. Kanninen and colleagues observed that Nrf2 activation in hippocampal neurons could effectively performed neuroprotective function [12]. Furthermore, it is considered that Nrf2 inducer modulates Nrf2 signaling particularly via astrocytes in the models of Parkinson's disease [66,67]. The cell type of Nrf2 activation in response to endogenous and exogenous stimuli in neurodegeneration need to be determined The mechanisms that underlie the decline in Nrf2 signalling with age and in AD progression remain to be elucidated. The potential role of Nrf2 in re-establishing oxidative-redox homeostasis once an initial insult has already occurred is an important area of investigation.

Meanwhile, dysregulated apoptosis is considered as an important pathogenic mechanism in AD due to the characteristic cell loss and tissue degeneration. Damaged and loss of neuronal cells are exhibited in the entorhinal cortex, hippocampus and neocortex-associated areas in the AD brain [68,69].

Increased p53 levels were observed in injured neurons of postmortem brain tissue from AD patients [70]. Enhanced p53 immunoreactivity along with an apoptosis marker was present in mouse brains overexpressing Aβ1-42 [71]. p53 activation has been proposed to correlate with the severity of the apoptosis insult [72]. IASPP, unlike the function of two other members of the ASPP family, is a conserved inhibitor of p53 [73]. Based on the roles of p53 in cancer prevention, research on iASPP function has mainly focused on cellular invasiveness, tumour occurrence and cancer progression [74,75]. Interestingly, iASPP could work as a binding partner of desmoplakin and desmin in cardiomyocytes. iASPP-deficient mice exhibit arrhythmogenic right ventricular cardiomyopathy and are vulnerable to sudden cardiac death [76]. In a rat model of acute optic nerve damage, upregulating iASPP expression could reduce retinal ganglion cell loss [21]. IASPP has been reported to suppress cellular senescence *in vitro* [77] and exert an antioxidant function independently of p53 [24]. Liu and colleagues observed that enhancing iASPP protein levels significantly reduced the infarction in a mouse model of focal cerebral ischaemia [20]. Importantly, an *in vitro* experiment demonstrated that iASPP competes with Nrf2 for interacting with Keap1 through a double glycine repeat domain; the binding of iASPP with Keap1 leads to the cytosolic accumulation of Nrf2 and facilitates Nrf2 nuclear translocation [24]. Given the increase in oxidative-redox imbalances and apoptosis in the AD brain, identifying a novel property of iASPP might provide a meaningful molecular explanation for AD progression. In this study, the expression of iASPP was lower in the APP/PS1 mouse brains than that of the age-matched WT brains. However, no significant differences in the protein expression or mRNA levels of ASPP1 and ASPP2 were detected between APP/PS1 and age-matched WT mouse brains. Syringin treatment reduced neuronal cell apoptosis in the APP/PS1 mouse brain. ChIP analysis showed that syringin did not alter the specific recruitment of p53 to the downstream genes, Bax and PUMA, suggesting that the syringin-induced apoptosis inhibition may be p53 independent.

Oxidative stress-induced apoptosis is considered a major common feature that integrates stress signalling. Ge and colleagues observed that overexpressing iASPP resulted in a significant decrease in ROS reduction in cancer cell lines *in vitro*. In contrast, iASPP siRNA induced ROS accumulation [24]. Upregulating iASPP expression by adeno-associated virus-iASPP intravitreal injections contributed to the survival of retinal ganglion cells in a mouse model of acute optic nerve damage [21]. The functional state of the endogenous defence system determines its capacity for resistance to oxidative stress damage. Nuclear Nrf2 levels affect the transcriptional activity of its target antioxidant genes. In the present study, the nuclear protein expression and DNA-binding activity of Nrf2 were lower in the APP/PS1 mouse brains than that of the age-matched WT control brains. Importantly, the cytosolic iASPP levels and iASPP-Keap1 interactions were markedly lower in the APP/PS1 mouse brains than those of the WT mouse brains. These findings suggested that the iASPP decline might be involved in the Nrf2 signalling impairment in the APP/PS1 mouse brain. Co-IP assays showed that syringin treatment increased the cytosolic iASPP protein levels and iASPP-Keap1 interactions, likely enhancing the competition of iASPP

with Nrf2 to bind Keap1 compared with that in the APP/PS1 mice not given syringin. GSH/GSSG, one of prominent index indicating oxidative-redox status, were significantly increased under syringin management in both WT and APP/PS1 mouse brains compared to those of their vehicle controls in our study. Nrf2 modulates the synthesis and regeneration of GSH [78], which is important for cell survival. Nrf2 inducer could regulate GSH levels in neurons and astrocytes [79]. Nrf2-mediated transcriptional activation of antioxidant genes in astrocytes may facilitate the biosynthesis of GSH, sustaining the redox status of neurons [80]. Further exploring the relationship of Nrf2 signal variation between neurons and astrocytes in AD progression is helpful in restoring redox balance with antioxidants in the AD intervention.

It has been reported that Nrf2 inducer, sulforaphane, could reduce BACE1 expression and subsequently Aβ production [81]. In our study, syringin treatment-caused upregulation of Nrf2 led to the decreases of β- and γ-secretases activities related to APP processing without altering their protein expression, reducing the Aβ deposition. The effects of syringin on regulating iASPP/Nrf2 axis were confirmed in APPswe cells *in vitro*. A preconditioning protocol was performed in our experiment. The cells were first treated with syringin for 6 h, and were followed by the incubation with H_2O_2 for 24 h. Syringin management protected APPswe cells against chronic H_2O_2 treatment-induced apoptosis and reduced ROS levels. The results suggest that syringin might offer enhanced antioxidant defenses in a preconditioning framework. The opinion that general preconditioning signals contribute to cellular protection is recognized [82–84]. H_2O_2-primed increases in Aβ secretions were reduced under syringin treatment in the APPswe cells, indicating that syringin-restored antioxidative activity reduced amyloidosis. Interestingly, iASPP siRNA abrogated the syringin-mediated Nrf2 upregulation and ROS reduction. Furthermore, syringin- or LV-iASPP-mediated iASPP increases facilitated NQO1 and γGCL-C transcription, but the effects were abrogated by Nrf2 siRNA or trigonelline (Nrf2 inhibitor).

5. Conclusions

Our *ex vivo* and *in vitro* findings addressed the neuroprotective effects of syringin against oxidative injury in AD model through competing with Nrf2 for Keap1, stabilizing Nrf2 and facilitating the antioxidative gene transcription (Fig. 8). Although the present experiments using the APP/PS1 mouse model and APPswe cells exhibit some certain limitations with respect to direct comparisons with the condition of the AD brain, our results demonstrate that iASPP decline is involved in Nrf2 degradation, contributing to the impairment of antioxidative defence in the development and progression of amyloid-related pathology. Further study on human AD postmortem brain tissue will contribute to revealing

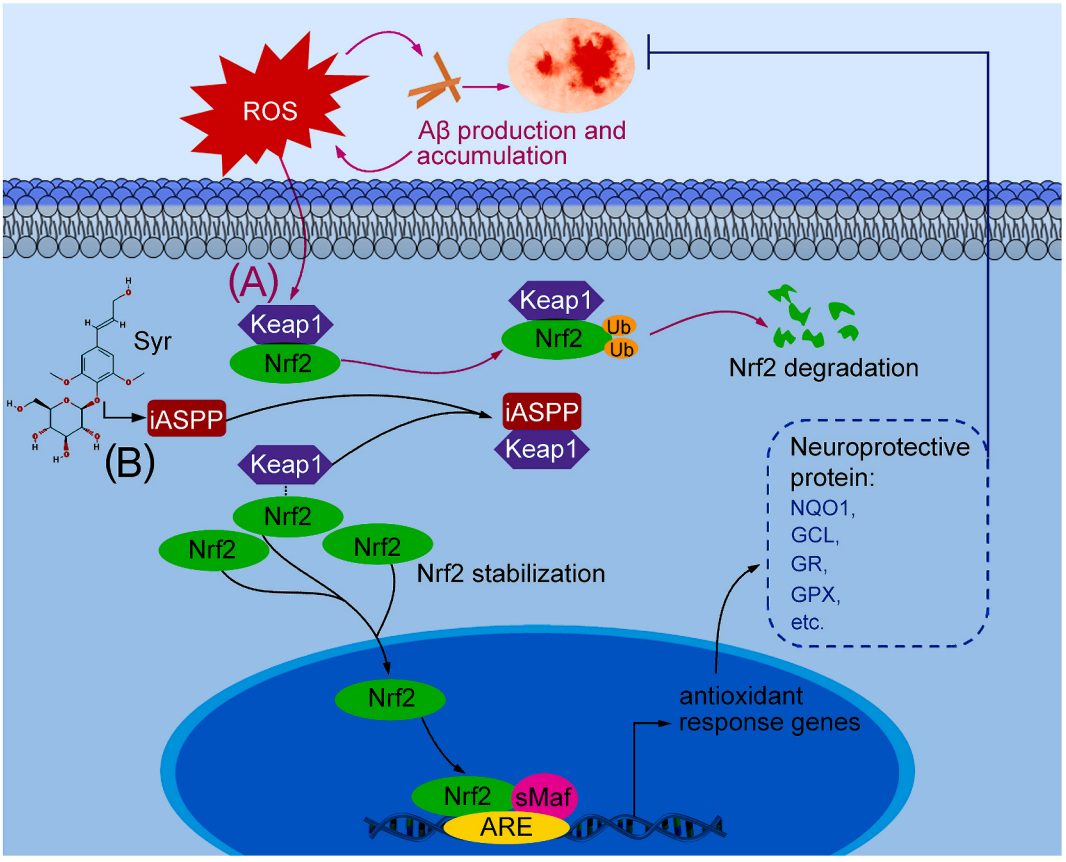

Fig. 8. Graphical abstract illustrates the possible neuroprotective mechanisms of syringin against AD-related neurodegeneration *via* iASPP/Nrf2 axis. Under physiological conditions, nuclear factor-erythroid 2-related factor 2 (Nrf2) Nrf2 interacts with Kelch-like ECH-associated protein 1 (KEAP1) in the cytoplasm and undergoes degradation by the proteasome through ubiquitination. Mild reactive oxygen species (ROS) production could induce Nrf2 release from Keap1 and facilitate it nuclear translocation, initiating transcription of antioxidative genes. (**A**) In Alzheimer's disease (AD) brain, Nrf2 signalling is decline. Chronic oxidative stress is related to the excessive generation of ROS, which facilitate progressive production and accumulation of β-amyloid (Aβ). The processing of Aβ aggregation further deteriorates oxidative imbalance. Higher proteasomal degradation of Nrf2 might worsen the poor antioxidant levels in AD brain. (**B**) Syringin (Syr) interacts with inhibitor of apoptosis-stimulating protein of p53 (iASPP), and increases the expression and activity of iASPP. IASPP competes with Nrf2 for Keap1, leading to Nrf2 dissociated from Keap1. Nrf2 stabilization in cytosol facilitates it translocate into nucleus. In the nucleus, Nrf2 interacts with small musculoaponeurotic fibrosarcoma (sMaf) proteins, binding to the antioxidant response elements (ARE). The activation of Nrf2 initiates the gene expression such as NAD (P) H: quinone oxidoreductase 1 (NQO1), glutamyl cysteine ligase (GCL), glutathione reductase (GR), determination of glutathione peroxidase (GPX), etc., playing the neuroprotective roles in ameliorating the AD-related pathology.

the direct effects of iASPP on the activity of Nrf2 signalling in AD pathology. Herein, our data show that syringin reduces oxidative stress, alleviates AD-related pathology, and upregulates Nrf2 signalling, which is involved in the enhancement of syringin-mediated iASPP-Keap1 interactions. Computational docking model data showed the direct binding of iASPP with syringin. Further study on the syringin-iASPP interactions may help in understanding the regulatory mechanism and designing novel potent modulators. Therefore, syringin might be a potential candidate for AD treatment.

Funding

This work was funded by the Natural Science Foundation of China (Nos. 81671041, 81971026), Natural Science Foundation of Liaoning Provincial Science & Technology Department in China (Nos. 2018225086, 20180550924), Natural Science Foundation of Jilin Provincial Educational Department in China (No. JJKH20200455KJ).

Authors' contributions

C. Y. Wang designed the study. C. Y. Wang, Q. Zhang, Z. Xun, L. Yuan, R. Li, X. Li and S.Y. Tian performed the experiments. R. Li, L. Yuan, X. Li, S.Y. Tian, N. Xin and Y. Xu analysed the data. C. Y. Wang and Q. Zhang wrote the manuscript. All authors concurred with the submission and approved the final version of the manuscript.

Declaration of competing interest

The authors declare that they have no conflict of interest.

Appendix A. Supplementary data

Supplementary data to this article can be found online at https://doi.org/10.1016/j.redox.2020.101672.

References

[1] G. Nesi, S. Sestito, M. Digiacomo, S. Rapposelli, Oxidative stress, mitochondrial abnormalities and proteins deposition: multitarget approaches in Alzheimer's disease, Curr. Top. Med. Chem. 17 (2017) 3062–3079.
[2] M.A. Ansari, S.W. Scheff, Oxidative stress in the progression of Alzheimer disease in the frontal cortex, J. Neuropathol. Exp. Neurol. 69 (2010) 155–167.
[3] D. Boche, E. Zotova, R.O. Weller, S. Love, J.W. Neal, R.M. Pickering, D. Wilkinson, C. Holmes, J.A. Nicoll, Consequence of Abeta immunization on the vasculature of human Alzheimer's disease brain, Brain 131 (2008) 3299–3310.
[4] M.T. Heneka, M.P. Kummer, A. Stutz, A. Delekate, S. Schwartz, A. Vieira-Saecker, A. Griep, D. Axt, A. Remus, T.C. Tzeng, E. Gelpi, A. Halle, M. Korte, E. Latz, D. T. Golenbock, NLRP3 is activated in Alzheimer's disease and contributes to pathology in APP/PS1 mice, Nature 493 (2013) 674–678.
[5] T.W. Kensler, N. Wakabayashi, S. Biswal, Cell survival responses to environmental stresses via the Keap1-Nrf2-ARE pathway, Annu. Rev. Pharmacol. Toxicol. 47 (2007) 89–116.
[6] M. McMahon, K. Itoh, M. Yamamoto, J.D. Hayes, Keap1-dependent proteasomal degradation of transcription factor Nrf2 contributes to the negative regulation of antioxidant response element-driven gene expression, J. Biol. Chem. 278 (2003) 21592–21600.
[7] A. Kobayashi, M.I. Kang, H. Okawa, M. Ohtsuji, Y. Zenke, T. Chiba, K. Igarashi, M. Yamamoto, Oxidative stress sensor Keap1 functions as an adaptor for Cul3-based E3 ligase to regulate proteasomal degradation of Nrf2, Mol. Cell Biol. 24 (2004) 7130–7139.
[8] X. He, M.G. Chen, G.X. Lin, Q. Ma, Arsenic induces NAD(P)H-quinone oxidoreductase I by disrupting the Nrf2 x Keap1 x Cul3 complex and recruiting Nrf2 x Maf to the antioxidant response element enhancer, J. Biol. Chem. 281 (2006) 23620–23631.
[9] B. Eftekharzadeh, N. Maghsoudi, F. Khodagholi, Stabilization of transcription factor Nrf2 by tBHQ prevents oxidative stress-induced amyloid beta formation in NT2N neurons, Biochimie 92 (2010) 245–253.
[10] C.P. Ramsey, C.A. Glass, M.B. Montgomery, K.A. Lindl, G.P. Ritson, L.A. Chia, R. L. Hamilton, C.T. Chu, K.L. Jordan-Sciutto, Expression of Nrf2 in neurodegenerative diseases, J. Neuropathol. Exp. Neurol. 66 (2007) 75–85.
[11] K. Kanninen, T.M. Malm, H.K. Jyrkkanen, G. Goldsteins, V. Keksa-Goldsteine, H. Tanila, M. Yamamoto, S. Yla-Herttuala, A.L. Levonen, J. Koistinaho, Nuclear factor erythroid 2-related factor 2 protects against beta amyloid, Mol. Cell. Neurosci. 39 (2008) 302–313.
[12] K. Kanninen, R. Heikkinen, T. Malm, T. Rolova, S. Kuhmonen, H. Leinonen, S. Yla-Herttuala, H. Tanila, A.L. Levonen, M. Koistinaho, J. Koistinaho, Intrahippocampal injection of a lentiviral vector expressing Nrf2 improves spatial learning in a mouse model of Alzheimer's disease, Proc. Natl. Acad. Sci. U.S.A. 106 (2009) 16505–16510.
[13] C.Y. Wang, Y. Xu, X. Wang, C. Guo, T. Wang, Z.Y. Wang, Dl-3-n-Butylphthalide inhibits NLRP3 inflammasome and mitigates alzheimer's-like pathology via nrf2-TXNIP-TrX Axis, Antioxid. Redox Signal 30 (2019) 1411–1431.
[14] D. Bergamaschi, Y. Samuels, B. Jin, S. Duraisingham, T. Crook, X. Lu, ASPP1 and ASPP2: common activators of p53 family members, Mol. Cell Biol. 24 (2004) 1341–1350.
[15] D. Bergamaschi, Y. Samuels, A. Sullivan, M. Zvelebil, H. Breyssens, A. Bisso, G. Del Sal, N. Syed, P. Smith, M. Gasco, T. Crook, X. Lu, iASPP preferentially binds p53 proline-rich region and modulates apoptotic function of codon 72-polymorphic p53, Nat. Genet. 38 (2006) 1133–1141.
[16] D. Bergamaschi, Y. Samuels, N.J. O'Neil, G. Trigiante, T. Crook, J.K. Hsieh, D. J. O'Connor, S. Zhong, I. Campargue, M.L. Tomlinson, P.E. Kuwabara, X. Lu, iASPP oncoprotein is a key inhibitor of p53 conserved from worm to human, Nat. Genet. 33 (2003) 162–167.
[17] X. Zhang, M. Wang, C. Zhou, S. Chen, J. Wang, The expression of iASPP in acute leukemias, Leuk. Res. 29 (2005) 179–183.
[18] L. Jiang, M.K. Siu, O.G. Wong, K.F. Tam, X. Lu, E.W. Lam, H.Y. Ngan, X.F. Le, E. S. Wong, L.J. Monteiro, H.Y. Chan, A.N. Cheung, iASPP and chemoresistance in ovarian cancers: effects on paclitaxel-mediated mitotic catastrophe, Clin. Canc. Res. 17 (2011) 6924–6933.
[19] Z. Liu, X. Zhang, D. Huang, Y. Liu, L. Liu, G. Li, Y. Dai, H. Tan, J. Xiao, Y. Tian, Elevated expression of iASPP in head and neck squamous cell carcinoma and its clinical significance, Med. Oncol. 29 (2012) 3381–3388.
[20] X. Liu, F. Li, S. Zhao, Y. Luo, J. Kang, H. Zhao, F. Yan, S. Li, X. Ji, MicroRNA-124-mediated regulation of inhibitory member of apoptosis-stimulating protein of p53 family in experimental stroke, Stroke 44 (2013) 1973–1980.
[21] A.M. Wilson, V.A. Chiodo, S.L. Boye, N.C. Brecha, W.W. Hauswirth, A. Di Polo, Inhibitor of apoptosis-stimulating protein of p53 (iASPP) is required for neuronal survival after axonal injury, PloS One 9 (2014). Article e94175.
[22] X. Liu, S. Wen, S. Zhao, F. Yan, D. Wu, X. Ji, Mild therapeutic hypothermia protects the brain from ischemia/reperfusion injury through upregulation of iASPP, Aging Dis. 9 (2018) 401–411.
[23] H. Yi, Y. Huang, F. Yang, W. Liu, S. He, X. Hu, MicroRNA-182 aggravates cerebral ischemia injury by targeting inhibitory member of the ASPP family (iASPP), Arch. Biochem. Biophys. 620 (2017) 52–58.
[24] W. Ge, K. Zhao, X. Wang, H. Li, M. Yu, M. He, X. Xue, Y. Zhu, C. Zhang, Y. Cheng, S. Jiang, Y. Hu, iASPP is an antioxidative factor and drives cancer growth and drug resistance by competing with Nrf2 for Keap1, Bind. Canc. Cell 32 (2017) 561–573.
[25] S. Lee, D. Son, J. Ryu, Y.S. Lee, S.H. Jung, J. Kang, S.Y. Lee, H.S. Kim, K.H. Shin, Anti-oxidant activities of Acanthopanax senticosus stems and their lignan components, Arch Pharm. Res. 27 (2004) 106–110.
[26] H.S. Niu, I.M. Liu, J.T. Cheng, C.L. Lin, F.L. Hsu, Hypoglycemic effect of syringin from Eleutherococcus senticosus in streptozotocin-induced diabetic rats, Planta Med. 74 (2008) 109–113.
[27] B. Kim, M.S. Kim, C.K. Hyun, Syringin attenuates insulin resistance via adiponectin-mediated suppression of low-grade chronic inflammation and ER stress in high-fat diet-fed mice, Biochem. Biophys. Res. Commun. 488 (2017) 40–45.
[28] X. Gong, L. Zhang, R. Jiang, C.D. Wang, X.R. Yin, J.Y. Wan, Hepatoprotective effects of syringin on fulminant hepatic failure induced by D-galactosamine and lipopolysaccharide in mice, J. Appl. Toxicol. 34 (2014) 265–271.
[29] J. Liu, Z. Zhang, Q. Guo, Y. Dong, Q. Zhao, X. Ma, Syringin prevents bone loss in ovariectomized mice via TRAF6 mediated inhibition of NF-kappaB and stimulation of PI3K/AKT, Phytomedicine 42 (2018) 43–50.
[30] D. Huang, Z. Hu, Z. Yu, Eleutheroside B or E enhances learning and memory in experimentally aged rats, Neural Regen. Res. 8 (2013) 1103–1112.
[31] E.J. Yang, S.I. Kim, H.Y. Ku, D.S. Lee, J.W. Lee, Y.S. Kim, Y.H. Seong, K.S. Song, Syringin from stem bark of Fraxinus rhynchophylla protects Abeta(25-35)-induced toxicity in neuronal cells, Arch Pharm. Res. 33 (2010) 531–538.
[32] W. Li, J. Yu, Y. Liu, X. Huang, N. Abumaria, Y. Zhu, W. Xiong, C. Ren, X.G. Liu, D. Chui, G. Liu, Elevation of brain magnesium prevents and reverses cognitive deficits and synaptic loss in Alzheimer's disease mouse model, J. Neurosci. 33 (2013) 8423–8441.
[33] C.Y. Wang, Z.Y. Wang, J.W. Xie, J.H. Cai, T. Wang, Y. Xu, X. Wang, L. An, CD36 upregulation mediated by intranasal LV-NRF2 treatment mitigates hypoxia-induced progression of Alzheimer's-like pathogenesis, Antioxidants Redox Signal. 21 (2014) 2208–2230.
[34] M. Costa-Mattioli, D. Gobert, H. Harding, B. Herdy, M. Azzi, M. Bruno, M. Bidinosti, C. Ben Mamou, E. Marcinkiewicz, M. Yoshida, H. Imataka, A. C. Cuello, N. Seidah, W. Sossin, J.C. Lacaille, D. Ron, K. Nader, N. Sonenberg, Translational control of hippocampal synaptic plasticity and memory by the eIF2alpha kinase GCN2, Nature 436 (2005) 1166–1173.
[35] M.Y. Lee, Y.H. Kuan, H.Y. Chen, T.Y. Chen, S.T. Chen, C.C. Huang, I.P. Yang, Y. S. Hsu, T.S. Wu, E.J. Lee, Intravenous administration of melatonin reduces the intracerebral cellular inflammatory response following transient focal cerebral ischemia in rats, J. Pineal Res. 42 (2007) 297–309.
[36] W.S. Juan, H.W. Lin, Y.H. Chen, H.Y. Chen, Y.C. Hung, S.H. Tai, S.Y. Huang, T. Y. Chen, E.J. Lee, Optimal Percoll concentration facilitates flow cytometric analysis for annexin V/propidium iodine-stained ischemic brain tissues, Cytometry A 81 (2012) 400–408.

[37] W.X. Zhong, Y.B. Wang, L. Peng, X.Z. Ge, J. Zhang, S.S. Liu, X.N. Zhang, Z. Xu H, Z. Chen, J.H. Luo, Lanthionine synthetase C-like protein 1 interacts with and inhibits cystathionine beta-synthase: a target for neuronal antioxidant defense, J. Biol. Chem. 287 (2012) 34189–34201.

[38] H. Wong, J. Levenga, P. Cain, B. Rothermel, E. Klann, C. Hoeffer, RCAN1 overexpression promotes age-dependent mitochondrial dysregulation related to neurodegeneration in Alzheimer's disease, Acta Neuropathol. 130 (2015) 829–843.

[39] D. Hu, F. Serrano, T.D. Oury, E. Klann, Aging-dependent alterations in synaptic plasticity and memory in mice that overexpress extracellular superoxide dismutase, J. Neurosci. 26 (2006) 3933–3941.

[40] C.Y. Wang, J.W. Xie, Y. Xu, T. Wang, J.H. Cai, X. Wang, B.L. Zhao, L. An, Z. Y. Wang, Trientine reduces BACE1 activity and mitigates amyloidosis via the AGE/RAGE/NF-kappaB pathway in a transgenic mouse model of Alzheimer's disease, Antioxid. Redox Signal 19 (2013) 2024–2039.

[41] K. Sahin, M. Tuzcu, H. Gencoglu, A. Dogukan, M. Timurkan, N. Sahin, A. Aslan, O. Kucuk, Epigallocatechin-3-gallate activates Nrf2/HO-1 signaling pathway in cisplatin-induced nephrotoxicity in rats, Life Sci. 87 (2010) 240–245.

[42] C.Y. Wang, Z.Y. Wang, J.W. Xie, T. Wang, X. Wang, Y. Xu, J.H. Cai, Dl-3-n-butylphthalide-induced upregulation of antioxidant defense is involved in the enhancement of cross talk between CREB and Nrf2 in an Alzheimer's disease mouse model, Neurobiol. Aging 38 (2016) 32–46.

[43] C. Alves da Costa, C. Sunyach, R. Pardossi-Piquard, J. Sevalle, B. Vincent, N. Boyer, T. Kawarai, N. Girardot, P. St George-Hyslop, F. Checler, Presenilin-dependent gamma-secretase-mediated control of p53-associated cell death in Alzheimer's disease, J. Neurosci. 26 (2006) 6377–6385.

[44] U.M. Moll, A. Zaika, Nuclear and mitochondrial apoptotic pathways of p53, FEBS Lett. 493 (2001) 65–69.

[45] J. Apelt, M. Bigl, P. Wunderlich, R. Schliebs, Aging-related increase in oxidative stress correlates with developmental pattern of beta-secretase activity and beta-amyloid plaque formation in transgenic Tg2576 mice with Alzheimer-like pathology, Int. J. Dev. Neurosci. 22 (2004) 475–484.

[46] M. Kowalska, K. Wize, M. Prendecki, M. Lianeri, W. Kozubski, J. Dorszewska, Genetic variants and oxidative stress in Alzheimer's disease, Curr. Alzheimer Res. 17 (2020) 208–223.

[47] J.M. Lee, M.J. Calkins, K. Chan, Y.W. Kan, J.A. Johnson, Identification of the NF-E2-related factor-2-dependent genes conferring protection against oxidative stress in primary cortical astrocytes using oligonucleotide microarray analysis, J. Biol. Chem. 278 (2003) 12029–12038.

[48] A. Lau, W. Tian, S.A. Whitman, D.D. Zhang, The predicted molecular weight of Nrf2: it is what it is not, Antioxid. Redox Signal 18 (2013) 91–93.

[49] S. Realmuto, A. Cinturino, V. Arnao, M.A. Mazzola, C. Cupidi, P. Aridon, P. Ragonese, G. Savettieri, M.D. Amelio, Tumor diagnosis preceding Alzheimer's disease onset: is there a link between cancer and Alzheimer's disease? J. Alzheimers Dis. 31 (2012) 177–182.

[50] A. Melo, L. Monteiro, R.M. Lima, D.M. Oliveira, M.D. Cerqueira, R.S. El-Bacha, Oxidative stress in neurodegenerative diseases: mechanisms and therapeutic perspectives, Oxid. Med. Cell Longev. (2011) 467180, 2011.

[51] O. Firuzi, R. Miri, M. Tavakkoli, L. Saso, Antioxidant therapy: current status and future prospect, Curr. Med. Chem. 18 (2011) 3871–3888.

[52] M. Concetta Scuto, C. Mancuso, B. Tomasello, M. Laura Ontario, A. Cavallaro, F. Frasca, L. Maiolino, A. Trovato Salinaro, E.J. Calabrese, V. Calabrese, Curcumin, hormesis and the nervous system, Nutrients 11 (2019) 2417, https://doi.org/10.3390/nu11102417.

[53] D. Pratico, K. Uryu, S. Leight, J.Q. Trojanoswki, V.M. Lee, Increased lipid peroxidation precedes amyloid plaque formation in an animal model of Alzheimer amyloidosis, J. Neurosci. 21 (2001) 4183–4187.

[54] H. Du, L. Guo, S. Yan, A.A. Sosunov, G.M. McKhann, S.S. Yan, Early deficits in synaptic mitochondria in an Alzheimer's disease mouse model, Proc. Natl. Acad. Sci. U.S.A. 107 (2010) 18670–18675.

[55] K. Ono, K. Hasegawa, H. Naiki, M. Yamada, Curcumin has potent anti-amyloidogenic effects for Alzheimer's beta-amyloid fibrils in vitro, J. Neurosci. Res. 75 (2004) 742–750.

[56] A.N. Begum, M.R. Jones, G.P. Lim, T. Morihara, P. Kim, D.D. Heath, C.L. Rock, M. A. Pruitt, F. Yang, B. Hudspeth, S. Hu, K.F. Faull, B. Teter, G.M. Cole, S. A. Frautschy, Curcumin structure-function, bioavailability, and efficacy in models of neuroinflammation and Alzheimer's disease, J. Pharmacol. Exp. Therapeut. 326 (2008) 196–208.

[57] Q.L. Ma, F. Yang, E.R. Rosario, O.J. Ubeda, W. Beech, D.J. Gant, P.P. Chen, B. Hudspeth, C. Chen, Y. Zhao, H.V. Vinters, S.A. Frautschy, G.M. Cole, Beta-amyloid oligomers induce phosphorylation of tau and inactivation of insulin receptor substrate via c-Jun N-terminal kinase signaling: suppression by omega-3 fatty acids and curcumin, J. Neurosci. 29 (2009) 9078–9089.

[58] A. Bilikiewicz, W. Gaus, Colostrinin (a naturally occurring, proline-rich, polypeptide mixture) in the treatment of Alzheimer's disease, J. Alzheimers Dis. 6 (2004) 17–26.

[59] S. Miquel, C. Champ, J. Day, E. Aarts, B.A. Bahr, M. Bakker, D. Banati, V. Calabrese, T. Cederholm, J. Cryan, L. Dye, J.A. Farrimond, A. Korosi, S. Laye, S. Maudsley, D. Milenkovic, M.H. Mohajeri, J. Sijben, A. Solomon, J.P.E. Spencer, S. Thuret, W. Vanden Berghe, D. Vauzour, B. Vellas, K. Wesnes, P. Willatts, R. Wittenberg, L. Geurts, Poor cognitive ageing: vulnerabilities, mechanisms and the impact of nutritional interventions Ageing, Res. Rev. 42 (2018) 40–55.

[60] T. Nguyen, P. Nioi, C.B. Pickett, The Nrf2-antioxidant response element signaling pathway and its activation by oxidative stress, J. Biol. Chem. 284 (2009) 13291–13295.

[61] K. Itoh, N. Wakabayashi, Y. Katoh, T. Ishii, K. Igarashi, J.D. Engel, M. Yamamoto, Keap1 represses nuclear activation of antioxidant responsive elements by Nrf2 through binding to the amino-terminal Neh2 domain, Genes Dev. 13 (1999) 76–86.

[62] S.S. Gounder, S. Kannan, D. Devadoss, C.J. Miller, K.J. Whitehead, S.J. Odelberg, M.A. Firpo, R. Paine, J.R. Hoidal, E.D. Abel, N.S. Rajasekaran, Impaired transcriptional activity of Nrf2 in age-related myocardial oxidative stress is reversible by moderate exercise training, PloS One 7 (2012). Article e45697.

[63] M.M. Rahman, G.P. Sykiotis, M. Nishimura, R. Bodmer, D. Bohmann, Declining signal dependence of Nrf2-MafS-regulated gene expression correlates with aging phenotypes, Aging Cell 12 (2013) 554–562.

[64] A.D. Kraft, J.M. Lee, D.A. Johnson, Y.W. Kan, J.A. Johnson, Neuronal sensitivity to kainic acid is dependent on the Nrf2-mediated actions of the antioxidant response element, J. Neurochem. 98 (2006) 1852–1865.

[65] A.I. Rojo, M. Pajares, P. Rada, A. Nunez, A.J. Nevado-Holgado, R. Killik, F. Van Leuven, E. Ribe, S. Lovestone, M. Yamamoto, A. Cuadrado, NRF2 deficiency replicates transcriptomic changes in Alzheimer's patients and worsens APP and TAU pathology, Redox Biol. 13 (2017) 444–451.

[66] J.R. Liddell, Are astrocytes the predominant cell type for activation of Nrf2 in aging and neurodegeneration? Antioxidants (Basel) (2017) 6, https://doi.org/10.3390/antiox6030065.

[67] A. Jazwa, A.I. Rojo, N.G. Innamorato, M. Hesse, J. Fernandez-Ruiz, A. Cuadrado, Pharmacological targeting of the transcription factor Nrf2 at the basal ganglia provides disease modifying therapy for experimental parkinsonism, Antioxid. Redox Signal 14 (2011) 2347–2360.

[68] G. Simic, I. Kostovic, B. Winblad, N. Bogdanovic, Volume and number of neurons of the human hippocampal formation in normal aging and Alzheimer's disease, J. Comp. Neurol. 379 (1997) 482–494.

[69] P.H. Axelsen, H. Komatsu, I.V. Murray, Oxidative stress and cell membranes in the pathogenesis of Alzheimer's disease, Physiology (Bethesda) 26 (2011) 54–69.

[70] S.M. de la Monte, Y.K. Sohn, J.R. Wands, Correlates of p53- and Fas (CD95)-mediated apoptosis in Alzheimer's disease, J. Neurol. Sci. 152 (1997) 73–83.

[71] F.M. LaFerla, C.K. Hall, L. Ngo, G. Jay, Extracellular deposition of beta-amyloid upon p53-dependent neuronal cell death in transgenic mice, J. Clin. Invest. 98 (1996) 1626–1632.

[72] C. Culmsee, M.P. Mattson, p53 in neuronal apoptosis, Biochem. Biophys. Res. Commun. 331 (2005) 761–777.

[73] G. Lettre, E.A. Kritikou, M. Jaeggi, A. Calixto, A.G. Fraser, R.S. Kamath, J. Ahringer, M.O. Hengartner, Genome-wide RNAi identifies p53-dependent and -independent regulators of germ cell apoptosis in C. elegans, Cell Death Differ 11 (2004) 1198–1203.

[74] J. Chen, F. Xie, L. Zhang, W.G. Jiang, iASPP is over-expressed in human non-small cell lung cancer and regulates the proliferation of lung cancer cells through a p53 associated pathway, BMC Canc. 10 (2010), https://doi.org/10.1186/1471-2407-10-694.

[75] E.V. Morris, L. Cerundolo, M. Lu, C. Verrill, F. Fritzsche, M.J. White, G. N. Thalmann, C.S. ten Donkelaar, I. Ratnayaka, V. Salter, F.C. Hamdy, X. Lu, R. J. Bryant, Nuclear iASPP may facilitate prostate cancer progression, Cell Death Dis. 5 (2014). Article e1492.

[76] M. Notari, Y. Hu, G. Sutendra, Z. Dedeic, M. Lu, L. Dupays, A. Yavari, C.A. Carr, S. Zhong, A. Opel, A. Tinker, K. Clarke, H. Watkins, D.J. Ferguson, D.P. Kelsell, S. de Noronha, M.N. Sheppard, M. Hollinshead, T.J. Mohun, X. Lu iASPP, A previously unidentified regulator of desmosomes, prevents arrhythmogenic right ventricular cardiomyopathy (ARVC)-induced sudden death, Proc. Natl. Acad. Sci. U.S.A. 112 (2015) E973–E981.

[77] M. Notari, Y. Hu, S. Koch, M. Lu, I. Ratnayaka, S. Zhong, C. Baer, A. Pagotto, R. Goldin, V. Salter, E. Candi, G. Melino, X. Lu, Inhibitor of apoptosis-stimulating protein of p53 (iASPP) prevents senescence and is required for epithelial stratification, Proc. Natl. Acad. Sci. U.S.A. 108 (2011) 16645–16650.

[78] Y. Chen, Y. Xu, H. Zheng, J. Fu, Y. Hou, H. Wang, Q. Zhang, M. Yamamoto, J. Pi, The role of nuclear factor E2-Related factor 2 and uncoupling protein 2 in glutathione metabolism: evidence from an in vivo gene knockout study, Biochem. Biophys. Res. Commun. 478 (2016) 87–92.

[79] S. Lavoie, Y. Chen, T.P. Dalton, R. Gysin, M. Cuenod, P. Steullet, K.Q. Do, Curcumin, quercetin, and tBHQ modulate glutathione levels in astrocytes and neurons: importance of the glutamate cysteine ligase modifier subunit, J. Neurochem. 108 (2009) 1410–1422.

[80] J.P. Bolanos, Bioenergetics and redox adaptations of astrocytes to neuronal activity, J. Neurochem. 139 (Suppl 2) (2016) 115–125.

[81] G. Bahn, J.S. Park, U.J. Yun, Y.J. Lee, Y. Choi, S.H. Baek, B.Y. Choi, Y.S. Cho, H. K. Kim, J. Han, J.H. Sul, S.H. Baik, J. Lim, N. Wakabayashi, S.H. Bae, J.W. Han, T. V. Arumugam, M.P. Mattson, D.G. Jo NRF2/ARE pathway negatively regulates BACE1 expression and ameliorates cognitive deficits in mouse Alzheimer's models, Proc. Natl. Acad. Sci. U.S.A. 116 (2019) 12516–12523.

[82] E.J. Calabrese, V. Calabrese, A. Tsatsakis, J.J. Giordano, Hormesis and Ginkgo biloba (GB): numerous biological effects of GB are mediated via hormesis, Ageing Res. Rev. (2020) 101019, https://doi.org/10.1016/j.arr.2020.101019.

[83] V. Calabrese, A. Santoro, A. Trovato Salinaro, S. Modafferi, M. Scuto, F. Albouchi, D. Monti, J. Giordano, M. Zappia, C. Franceschi, E.J. Calabrese, Hormetic approaches to the treatment of Parkinson's disease: perspectives and possibilities, J. Neurosci. Res. 96 (2018) 1641–1662.

[84] V. Calabrese, C. Cornelius, A.T. Dinkova-Kostova, E.J. Calabrese, M.P. Mattson, Cellular stress responses, the hormesis paradigm, and vitagenes: novel targets for therapeutic intervention in neurodegenerative disorders, Antioxidants Redox Signal. 13 (2010) 1763–1811.